Effects of galaxy interactions on their central B/P/X/bl structures

Riku Rautio
Astronomy
February 27, 2019

Contents

1 Introduction

The origin and physical character of the bulges of spiral galaxies is an essential and long debated part of the theory of galaxy formation and evolution. The classical view has been that the bulges are relaxed, velocity dispersion supported structures, so called classical bulges. Classical bulges are thought to be formed at high redshifts as a results of some violent, catastrophic events, such as monolithic collapses (Eggen et al., 1962) or galaxy mergers (White & Rees, 1978), in a manner similar to that usually prescribed to elliptical galaxies as a whole. A

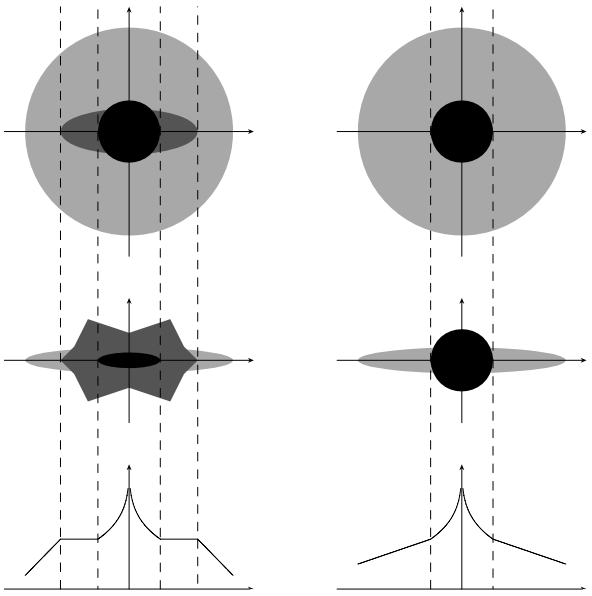

Figure 1: Cartoon depicting models for a galaxy with a B/P bulge (left) and a galaxy with a classical bulge (right). At the top are the face-on views, at the middle the edge-on views, and at the bottom the edge-on surface brightness profiles. The galaxy in the right consists of a classical bulge within a thin exponential disc. The galaxy in the left consists of a thin inner disc component with a steep surface brightness profile (discy pseudobulge), a B/P bulge, and an outer exponential disc. This cartoon is somewhat outdated, as in the current model of a galaxy with a composite bulge, the B/P feature extends only for half the length of the thin bar visible face-on. Figure taken from Bureau et al. (2006).

more modern development has been the identification of finer structure and rotation in the bulges of nearby disc galaxies. Nowadays bulges are often divided to three distinct classes: classical bulges, discy pseudobulges and Boxy/Peanut (B/P) bulges (Athanassoula, 2005).

Pseudobulges, including both the discy pseudobulges and the B/P bulges, are rotationally supported structures (Kormendy & Illingworth, 1982), formed out of the disc material by secular evolutionary processes. Discy pseudobulges appear as flat structures in the central parts of the discs, that have excess light above the exponential disc in the surface brightness profile. They are essentially miniature discs embedded in the main disc. B/P bulges are bar related structures with boxy, peanut or X-shape morphologies, easily visible in edge-on view. Figure 1 shows a cartoon depiction of a galaxy with a composite bulge consisting of both a discy pseudobulge and a B/P bulge, compared to a galaxy with only a classical bulge.

Boxy/Peanut bulges have been found to be present in many if not most of

the nearby spiral galaxies (e.g. Lütticke, Dettmar, & Pohlen 2000), and as such they are a very important piece of the puzzle of galaxy formation and evolution. They have long been associated with bars (Combes & Sanders, 1981), and can even be thought of as the thick inner part of the bar (Athanassoula, 2005). The theoretical reason behind the shape of the B/P bulge has been shown to be that the vertical resonances with the bar maintain the orbits of stars that make up the B/P bulge (the x1v1 orbital family; Skokos et al. 2002). The problem with the study of B/P bulges has been the difficulty in identifying them in face-on galaxies, as the B/P structure is only visible edge-on. While bars have often been used as proxies of B/P bulges in face-on galaxies, it is only the vertically narrow, easily distinguishable part of the bar that is seen, which is not the same vertically thick part that makes up the B/P bulge. It is currently not known if all thin bars host a B/P bulge.

A new morphological feature, a barlens (bl; Laurikainen et al. 2011) has been suggested by Laurikainen et al. (2014) as the potential face-on counterpart of B/P bulges. Barlenses are intermediate size lens-like components, associated with bars, that are visually similar to bulges. They typically cover half of the bar length, and smoothly blend with the bar, appearing as a single structure. The evidence suggesting a link between barlenses and B/P bulges include their colors and their cumulative stellar age and metallicity distributions, which have been shown to be similar to those of bars (Herrera-Endoqui et al., 2017; Laurikainen et al., 2018), and their surface brightness profiles, which correspond to those of simulated face-on B/P bulges (Athanassoula et al., 2015). Also, when B/P bulges are identified in nearly edge-on galaxies, and barlenses in less inclined galaxies, the combined sample of their host galaxies has a flat axial ratio distribution (Laurikainen et al., 2014). This is consistent with them representing a single population viewed at different inclinations.

Salo & Laurikainen (2017) showed that in *N*-body simulations the forming of a clean, round barlens requires a steeply rising rotation curve, while without that an X-shape feature is still seen even face-on. This is consistent with the observation that barlenses concentrate on earlier Hubble types (which have a higher central mass concentration compared to later Hubble types) than B/P bulges (Laurikainen et al., 2014). Figure 2 shows examples of simulated and real barlenses and X-shapes, while figure 3 shows the three dimensional structure of a simulated B/P bulge. It is clear that B/P bulges are highly complex and have varied structures, made up by many different orbital families, and we still do not fully understand their structure and development.

One way to gain information about the origin of these morphological structures is by studying interacting galaxies. It has been long known that interaction can greatly affect the observable properties of galaxies. Tidal effects of close encounters can cause narrow extended structures between two interacting galaxies

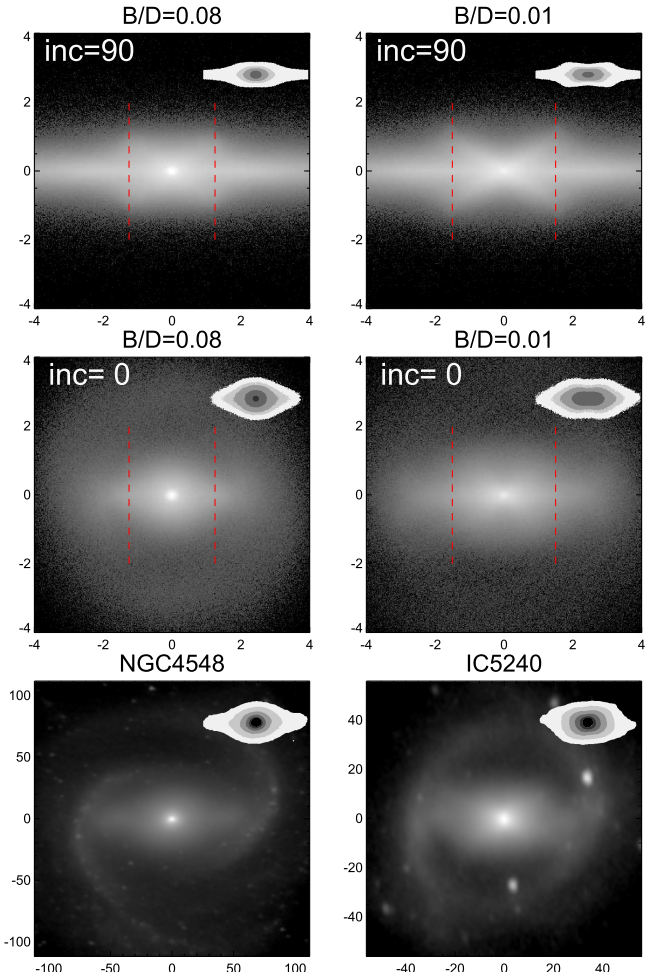

Figure 2: Two simulation models and two observational counterparts with B/P structures. The upper row shows the models seen edge-on and the middle row face-on. Both simulations have a small classical bulge, $B/D = 0.08$ for the left one and $B/D = 0.01$ for the right one. The small insert figures show isophotal contours of the central regions. In the model with the smaller classical bulge the X-shape is still visible in the face-on view (middle right figure). The bottom row shows deprojected images of NGC4548 (left, $i = 39°$, barlens) and IC5240 (right, $i = 44°$, X-shape). The axis units are in simulation units (initial scale lengths) for the models, and in arcseconds for the observed galaxies. Figure taken from Salo & Laurikainen (2017).

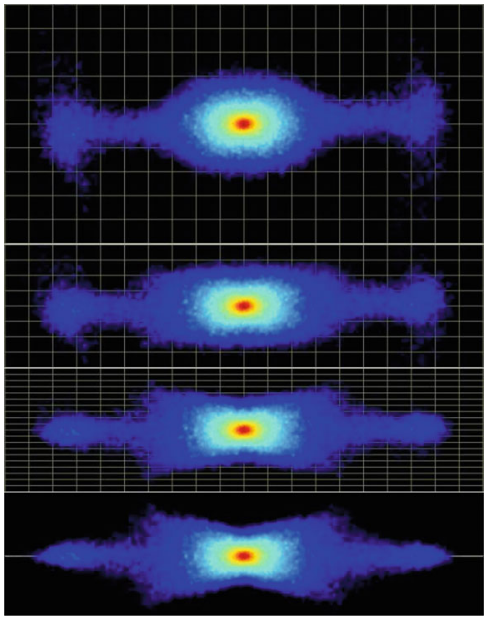

Figure 3: The isolated B/P structure of an *N*-body simulation seen perpendicular to bar major axis from different viewing elevations. The top panel shows a face-on view and the bottom panel a edge-on one, with two intermediate viewing elevations in the second and third panels. A Cartesian grid with 1 x 1 kpc cell size located on the equatorial plane is also shown in all panels. Figure taken from Athanassoula (2016).

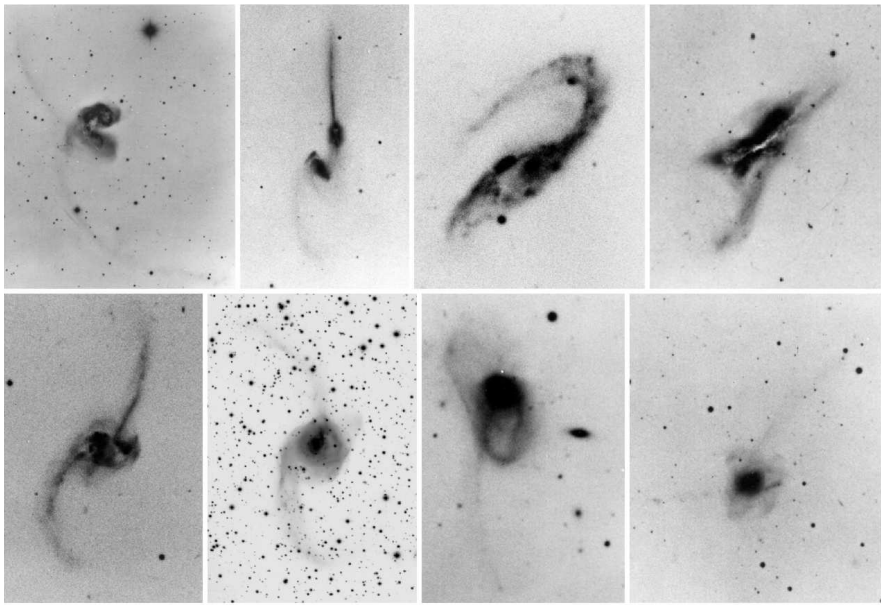

Figure 4: The Toomre's sequence of interacting galaxies. From left tor right, top: NGC4038/39, NGC4676, NGC3509, NGC0520; bottom: NGC2623, NGC3256, NGC3921, NGC7252. Figure taken from Duc & Renaud (2013).

(bridges), or opposite from each other (tails) (Toomre & Toomre, 1972). While the inner parts of the disc are more resistant to tidal effects than the outer parts, the gravity of a passing companion galaxy may still create asymmetries, or even create or amplify spiral arms (Toomre, 1981). Pronounced rings can be produced by collisions, when a companion passes through the disc plane of the victim (Few & Madore, 1986).

Mergers of galaxies can change their morphologies globally, sometimes even catastrophically. Mutual tidal capture, a major merger, of two disc galaxies of similar masses is classically thought to result in an elliptical galaxy (Toomre & Toomre, 1972). Accretion of less-massive neighbors, minor mergers, may cause relatively minor damage to the parent galaxy, while still causing changes to the structure in all parts of it, including the core. It can give rise to 'fine structures', such as shells, ripples, or plumes, in the parent galaxy (Hernquist & Quinn, 1988). Mass transfer or accretion may also create polar rings, i.e. rings that are perpendicular to the major axis of the disc (Athanassoula & Bosma, 1985). In addition, minor mergers of earlier stages may manifest as secondary nuclei, warps and disturbed discs. Figure 4 shows the Toomre's sequence, an evolutionary sequence of prototypical galaxies in different stages of merging process (Toomre, 1977).

What is the effect of interaction on B/P bulges? How strong interaction is required to destroy them? Weaker interaction may act as a trigger and a driver for

secular evolution, while major mergers should destroy most non-relaxed structures. There have been studies supporting both the ideas that interactions can induce bar formation (Noguchi, 1987; Pettitt & Wadsley, 2018), as well as impede it (Athanassoula, 2003; Moetazedian et al., 2017; Zana et al., 2018). X-shaped structures and boxy isophotes have also been linked to interactions (Hernquist & Quinn, 1989; Mihos et al., 1995). Recently Łokas et al. (2016) used *N*-body simulations of galaxies in clusters, and found that galaxies form more pronounced B/P bulges when tidal forces are stronger. The tidal and hydrodynamical forces present in galaxy interactions and mergers can clearly change and shape all structures of galaxies, and may even play a crucial part in formation for many of them. By studying the occurrence of B/P bulges in interacting, merger and peculiar galaxies, we will gain essential information about their nature.

In this thesis I use deep optical images to study what effects interactions between galaxies have on the B/P and bl structures. I classify a sample of 1413 galaxies according to their interactions and B/P structures, and examine the statistical differences between the different classes. For each galaxy I check if and how it is interacting, as well as mark down whether it has a barlens or X-shape structure. I use the X-shapes as a proxy of B/P bulges in edge-on galaxies, as they are easily distinguishable from unsharp masks, and present in most B/P bulges.

In section 2, I go over the sample and the methods used to identify the studied structures, with 2.1 focusing on the classification of interaction, and 2.2 on the barlenses and X-shapes. In section 3, I review the results of the study, with 3.1 explaining the general properties of the sample, 3.2 focusing on interacting galaxies, and 3.3 on mergers and peculiars. In section 4, I discuss the results, with 4.1 focusing on interpreting them, 4.2 evaluating their validity, and 4.3 examining some future prospects. I summarize and conclude the results in section 5.

2 Methods

The sample I use is drawn from the Southern Galactic Cap of the Sloan Digital Sky Survey (SDSS; Abazajian et al. 2009), or the Stripe 82. It is a 275 square degree region along the celestial equator ($-50° \leq RA \leq 60°$, $-1°.25 \leq Dec. \leq 1°.25$), imaged many times with the Sloan Foundation 2.5m Telescope. I chose a total of 1413 galaxies based on their apparent diameter, taking all the galaxies in the Stripe 82 region with apparent diameters in the 25 B-magnitude per square arcsecond surface brightness level (D25) larger than 0.5 arcminute, with the D25 taken from the Principal Galaxies Catalog (PGC; Paturel et al. 1989). This was chosen as the limit, as identification of barlenses and X-shapes for galaxies of smaller angular size would not be possible with the resolution reached by the images.

I used the deep IAC Stripe 82 co-add images by Fliri & Trujillo (2016) for

the visual identification of the studied features. Fliri & Trujillo used all 303 runs covering Stripe 82 from the seventh data release of Sloan Digital Sky Survey (SDSS DR7), reaching approximately 50 observation times for every region of Stripe 82. They reach 50 per cent point source completeness limits of 25.2, 24.7 and 24.3 mag, and have median full width at half maximum values of 1.24, 1.10 and 1.02 arcseconds for *g*, *r* and *i* bands respectively. The pixel size of the images is 0.396 arseconds.

The IAC Stripe 82 data was chosen because of the extreme depth reached by the co-adds. The co-adds were especially designed to preserve low-surface-brightness features. This allows for the detection of tidal tails, stellar streams and other low surface brightness features, making the data well suited for finding interactions between galaxies. Combining this with the restriction to sufficiently large angular size results in a sample where both external interactions and internal features like barlenses and X-shapes should be easily identifiable.

I used the *i*-band co-adds as well as the 'ultra-deep *r*-band' co-adds, which Fliri & Trujillo obtained by stacking of the *g*, *r* and *i* co-added images. I used *i*-band images in identifying the barlenses and X-shapes, as they are easiest to detect in *i*-band. I used 'ultra-deep *r*-band' images in identifying companions and interactions, as they reached the highest depth, useful for the identification of the low surface brightness features indicating interactions. For identifying the X-shapes, I made unsharp masks for the *i*-band images. The images I used for identification of interactions and X/bl features can be found in the web. Directions to the website are given at the end of this thesis.

Additional galaxy data was retrieved from HyperLEDA (Makarov et al., 2014), including the Hubble types, bar classifications and galaxy axis ratios. Inclinations were calculated for the galaxies according to equations 1 and 2, from the decimal logarithmic apparent axis ratios of the isophote 25 mag/arcsec^2 in the B-band ($logr25$ of HyperLEDA). In the equations a is the major axis length and b the minor axis length of the galaxy.

$$i = \arccos(b/a)\frac{180^\circ}{\pi} \tag{1}$$

$$b/a = (10^{logr25})^{-1} \tag{2}$$

2.1 Wide field images

For the study of interactions, I used the 'ultra-deep *r*-band' images by Fliri & Trujillo. I created 'postage stamp' images of the environments of my sample galaxies, scaling them to show a wide field of view, a 250 kpc sided square region centered on the studied galaxy. A large enough area was used to not miss any potential

companions. The distances of the galaxies were calculated from the radial velocities retrieved from HyperLEDA, using a Hubble constant of 71.9 $\mathrm{kms}^{-1}\mathrm{Mpc}^{-1}$.

Nearby galaxies, for which redshifts could be found, were identified in each of the images. For the identification, redshifts from the PGC, CfA Redshift Catalog (ZCAT; Huchra et al. 1999) and NASA-Sloan Atlas (NSA; Blanton et al. 2011) catalogs were used. Nearby galaxies with radial velocities within $\pm$1000 km/s from the target galaxy were marked in the image, and considered for possible interactions. The radii, radial velocities and *i*-band absolute magnitudes were taken from the aforementioned catalogs. The quality of the data varied between the catalogs, so for most parameters (coordinates, radii and radial velocities), priority was given to PGC and the data was chiefly taken from there, with NSA as the second choice. For the magnitudes however, the Sersic *i*-band absolute magnitudes [1] of NSA were preferred over PGC magnitudes, due to the importance of comparability of the magnitudes and the fact that PGC did not list most of the companion galaxies.

The Dahari Q parameter (Dahari, 1984) was also calculated for all of the companion galaxies, by calculating the fluxes from the absolute magnitudes and equating them to masses of the galaxies. Dahari Q parameter measures the strength of a tidal interaction caused by a companion galaxy, compared to the internal forces of the main galaxy. The equation for the Dahari Q parameter is given in equation 3, where F_{tidal} and $F_{central}$ are the tidal and internal forces affecting the main galaxy, m_{main} and $m_{companion}$ are the masses of the main and the companion galaxies, r_{main} is the radius (half of the D25) of the main galaxy, and d is the distance between the main and the companion galaxy. Equation 4 gives the relation between the mass ratio and absolute magnitudes, with f_{main} and $f_{companion}$ being the spectral flux densities, and M_{main} and $M_{companion}$ the absolute *i*-band magnitudes of the main and the companion galaxies.

$$Q_{Dahari} = \frac{F_{tidal}}{F_{central}} = \frac{m_{companion} \times r_{main}/d^3}{m_{main}/r_{main}^2} = \frac{m_{companion}}{m_{main}} \left(\frac{r_{main}}{d}\right)^3 \tag{3}$$

$$\frac{m_{companion}}{m_{main}} \approx \frac{f_{companion}}{f_{main}} = 10^{\frac{M_{main}-M_{companion}}{2.5}} \tag{4}$$

An interaction strength category was assigned to each of the main galaxies, based on the catalog data, as well as visual interpretation. The galaxies were assigned to one of the four categories:

- non-interacting

[1] Sersic absolute magnitudes are absolute magnitudes that are calculated from fluxes derived using a Sersic profile fit (Sérsic, 1963).

- interacting
- ongoing merger
- peculiar (merger remnant)

For a galaxy to be considered interacting, it had to be visibly disturbed by the tidal forces of its perceived neighbors. To avoid confusion with fore- or background galaxies these neighbors were required to have measured redshifts in one of the used catalogs, have a projected distance less than 250 kpc to the main galaxy and to be within $\pm$1000 km/s of it in recession velocity. Galaxies appearing within the considered area, but lacking redshifts, were ignored, except in the cases where the visual disturbance on the main galaxy was obvious. The Dahari Q parameters were also used to help the determination in a case by case basis. The median logarithmic Dahari Q parameter for the interacting galaxies was $\log Q_{Dahari} = -0.9$, compared to $\log Q_{Dahari} = -3.4$ for the non-interacting ones. Figure 5 shows two examples of interacting galaxies, while figure 6 shows two non-interacting galaxies.

Galaxy was assigned ongoing merger if its normal spiral and disc structure was completely broken and the merging companion, or companions, could still be differentiated from the main galaxy. For most of the merger class galaxies redshifts existed for both the main galaxy and its companion. While most of these galaxies were experiencing major mergers, some minor merger galaxies, where the lesser partner existed as a secondary nucleus within the spiral structure of the main galaxy, were also identified and categorized as ongoing mergers. The median logarithmic Dahari Q parameter was $\log Q_{Dahari} = 0.5$ for the ongoing mergers. Figures 7 and 9 show examples of mergers.

In literature the term peculiar galaxy can have many meanings, but here with the assignment peculiar, I mean a galaxy with an obviously disturbed morphology, similar to mergers, without any apparent companion visible. Additionally, galaxies with very heavy distortions and having only significantly smaller companions visible were considered peculiar, as it would be unlikely that the observed features would be solely caused by the small satellite companions. Features such as shells, tails and double nuclei were looked for. The assumption here is that these are galaxies in later stages of merger processes, or post-mergers. It should be noted that it is possible that for some of these galaxies the disturbance could be caused by a nearby companion without a redshift measurement that was discarded as a background galaxy. For the peculiars, the median logarithmic Dahari Q parameter was only $\log Q_{Dahari} = -3.3$. This is not a surprise as for most of the peculiars there existed redshifts for only a single galaxy, as the differentiation of the merging partners is impossible due to the advanced stage of the process. This means

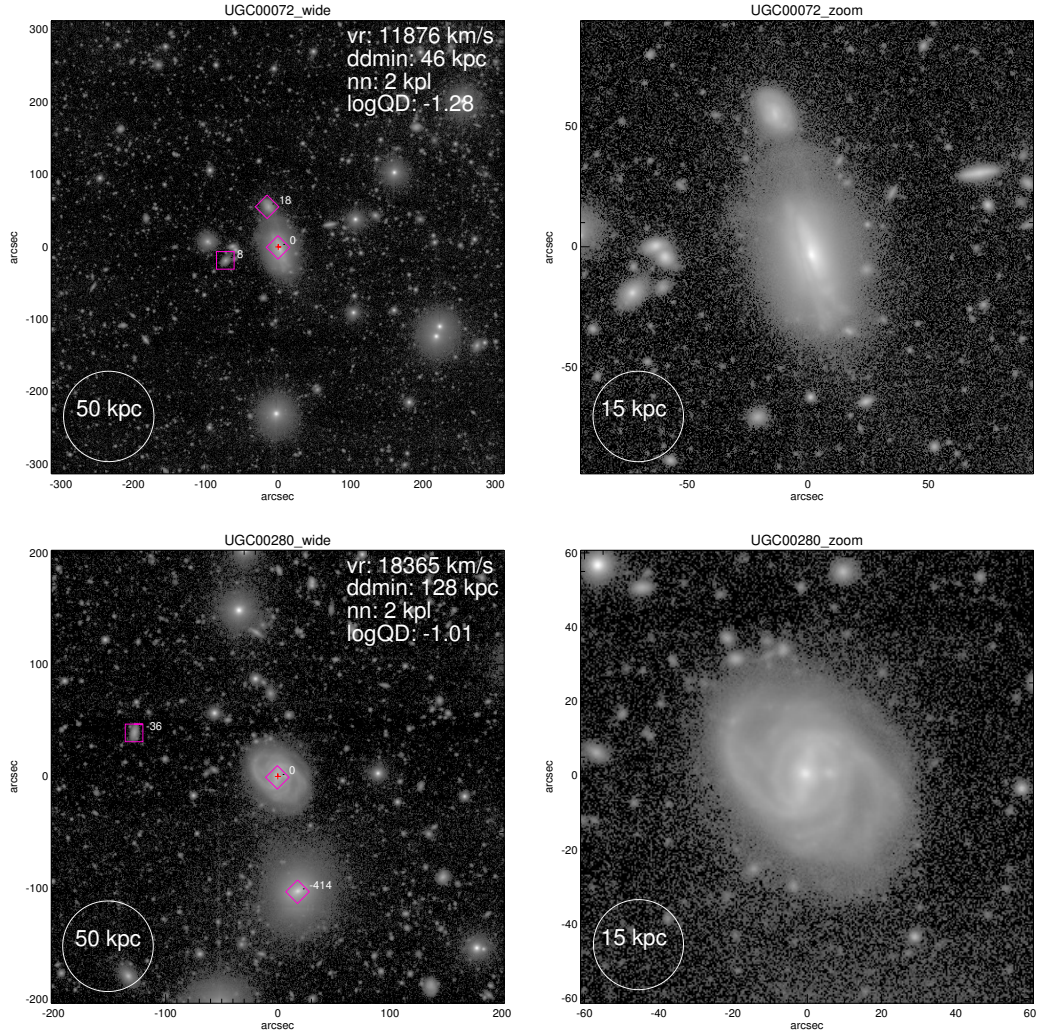

Figure 5: Two interacting galaxies, UGC00072 (upper row) and UGC00280 (lower row). Left images are the 'ultra-deep *r*-band' wide field 'postage stamp' images, showing a 250 kpc sided square region, and the right ones are the same image zoomed in to show a 75 kpc sided square region. The images reach a limit of 28.5 mag arcsec^{-2}. In the wide field images the galaxies' radial velocities, visual distance to the closest neighbor, number of nearby galaxies, and the logarithmic Dahari Q parameter of the closest neighbor are given. Also all nearby galaxies were marked on the images, diamonds indicating that the data of the companion galaxy was taken from the PGC, and squares indicating that it was taken from the NSA. The radial velocity difference (to the main galaxy) of each companion is written next to them. UGC00072 is clearly being disrupted by the satellite galaxy above it. The signs of interaction are subtler in UGC00280, but one can notice some asymmetry and stretching of the spiral arms on the side close to the nearby elliptical galaxy.

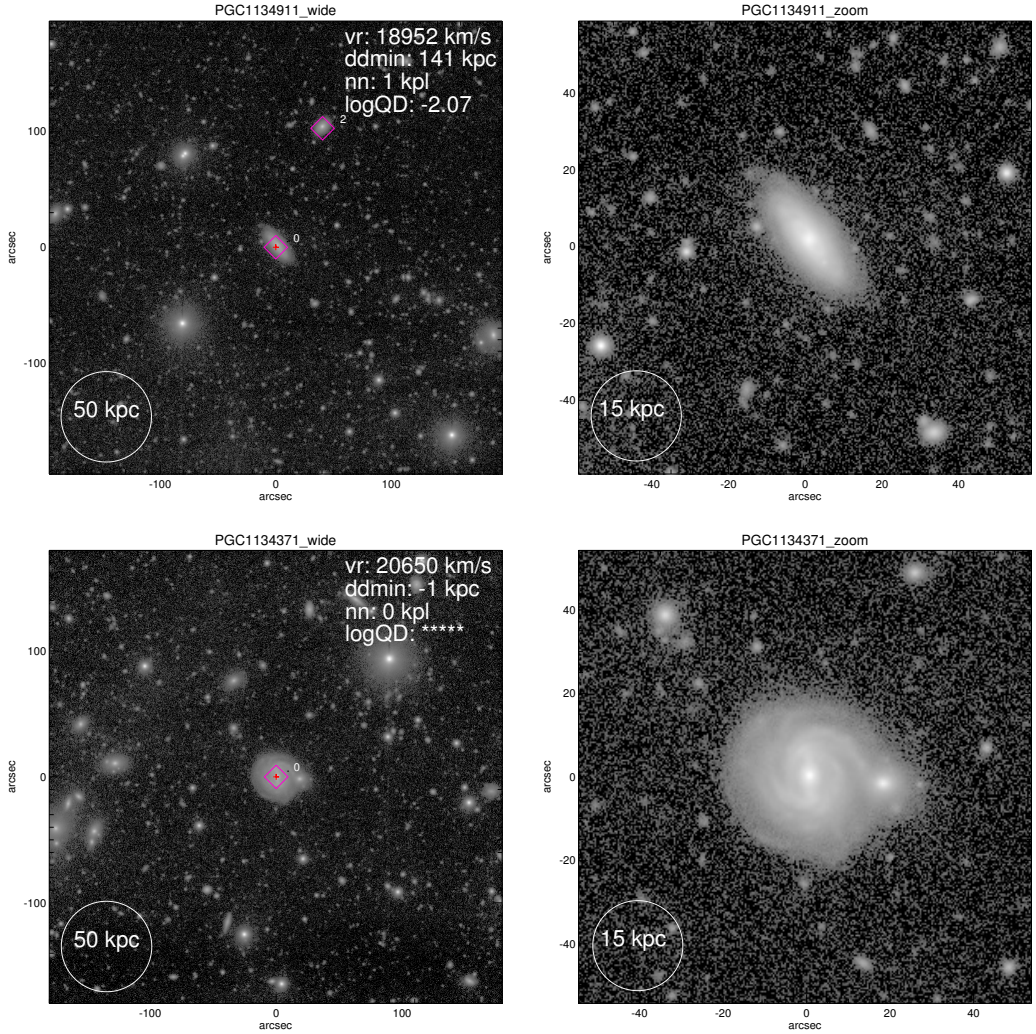

Figure 6: Two non-interacting galaxies, PGC1134911 (upper row) and PGC1134911 (lower row). PGC1134911 was classified as a non-interacting even though it has a relatively nearby companion, because it has no morphological indications of interaction. PGC1134371 looks to have a very close, even merging smaller companion. Still it was classified as non-interacting since the companion had a radial velocity that did not fit to the required $\pm$1000 km/s range, that is, being a fore- or background galaxy.

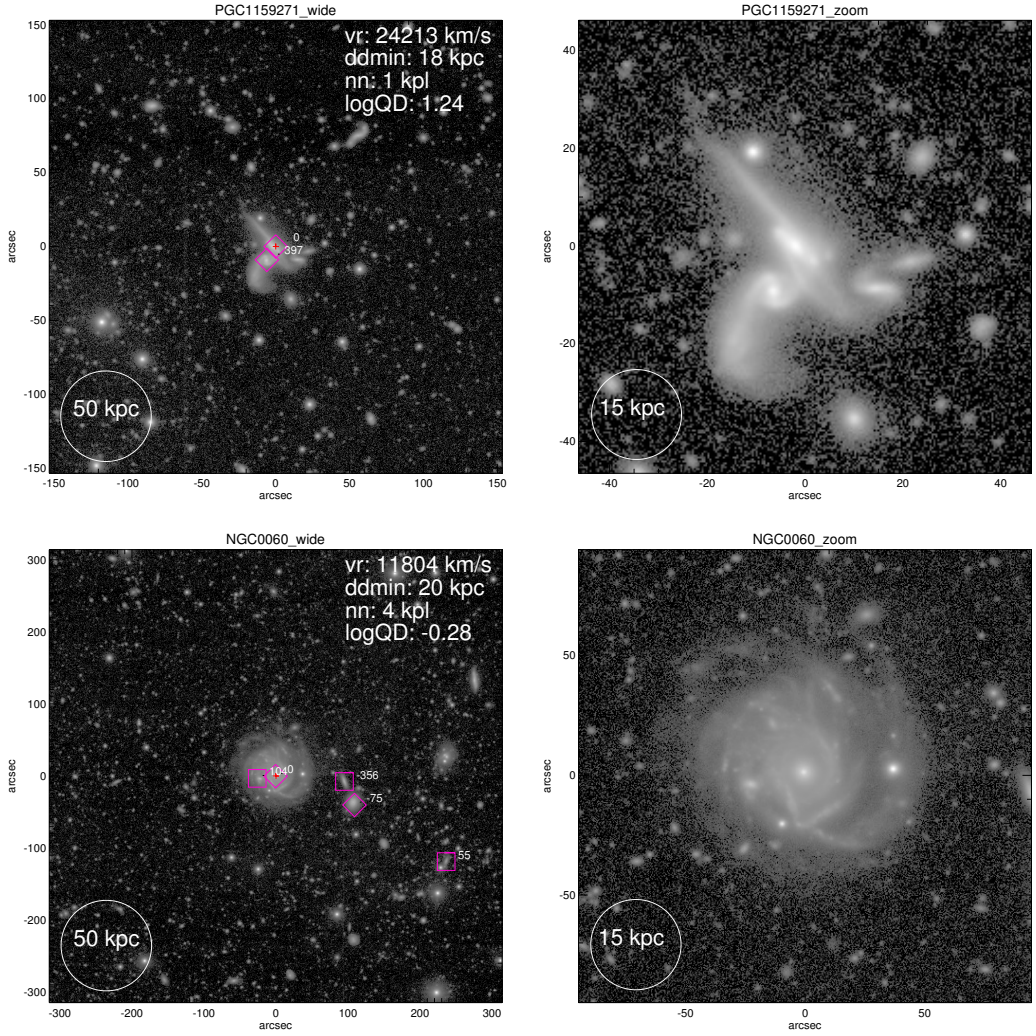

Figure 7: Two pairs of merger galaxies, PGC1159271 and PGC1159211 (upper row), and NGC0060 (lower row). PGC1159271 and PGC1159211 are undergoing an obvious major merger with each other. NGC0060 is undergoing a minor merger with a small companion that has already entered its disc. This is evident from the small radial velocity difference of 104 km/s of the companion as well as the heavy distortion in NGC0060 spiral structure.

that the Dahari Q parameter is calculated with the next closest galaxy, which may be far away. Figures 8 and 9 show examples of peculiars.

2.2 Unsharp mask images

Unsharp mask images were done for the *i*-band images, using the same methods as in Laurikainen & Salo (2017). First the images were convolved with a Gaussian kernel, then the original images were divided with the convolved images. The unsharp masked images were scaled to show a square region with sides twice the D25 diameter of the studied galaxy. These were used together with regular *i*-band images, scaled to show a square with sides four times the D25 diameter of the galaxy, for the identification of the studied internal features.

I looked for the different B/P features, barlenses and X-shapes, from the unsharp masked *i*-band images, identifying them by eye. While it is possible for an X-shape and a barlens to exist simultaneously in a galaxy, I did not consider such galaxies here, and instead identified any barlens galaxies with traces of X-shapes as just barlens galaxies. Each galaxy was assigned to one of the five categories:

- no X/bl features
- barlens
- clear X-shape
- unclear X-shape
- elliptical X-shape

While barlenses are visible both in the unsharp masked images as well as in the regular images, I preferred the regular *i*-band co-adds over the unsharp masks for their identification, as in some cases, especially in inclined galaxies, the unsharp masked image may show only an X-shape. So for a galaxy to be assigned a barlens, the feature had to be visible in the regular *i*-band image. Examples of barlenses are shown in figure 10.

I divided the X-shapes into clear X-shapes and unclear X-shapes. A galaxy was deemed to have a clear X-shape if it was an edge-on galaxy with a clear X-shape in the unsharp mask, and the X-shape was usually visible in the regular i-band image as well. The cases where the galaxy was inclined rather than edge-on, and the X-shape was less clear while still present in the unsharp masked images, were classified as unclear X-shapes. Figure 11 shows examples of clear X-shapes, while figure 12 shows examples of unclear ones.

Additionally, certain X-shape like features only visible on the unsharp masks of certain, mostly elliptical galaxies were identified, and designated as ‘elliptical

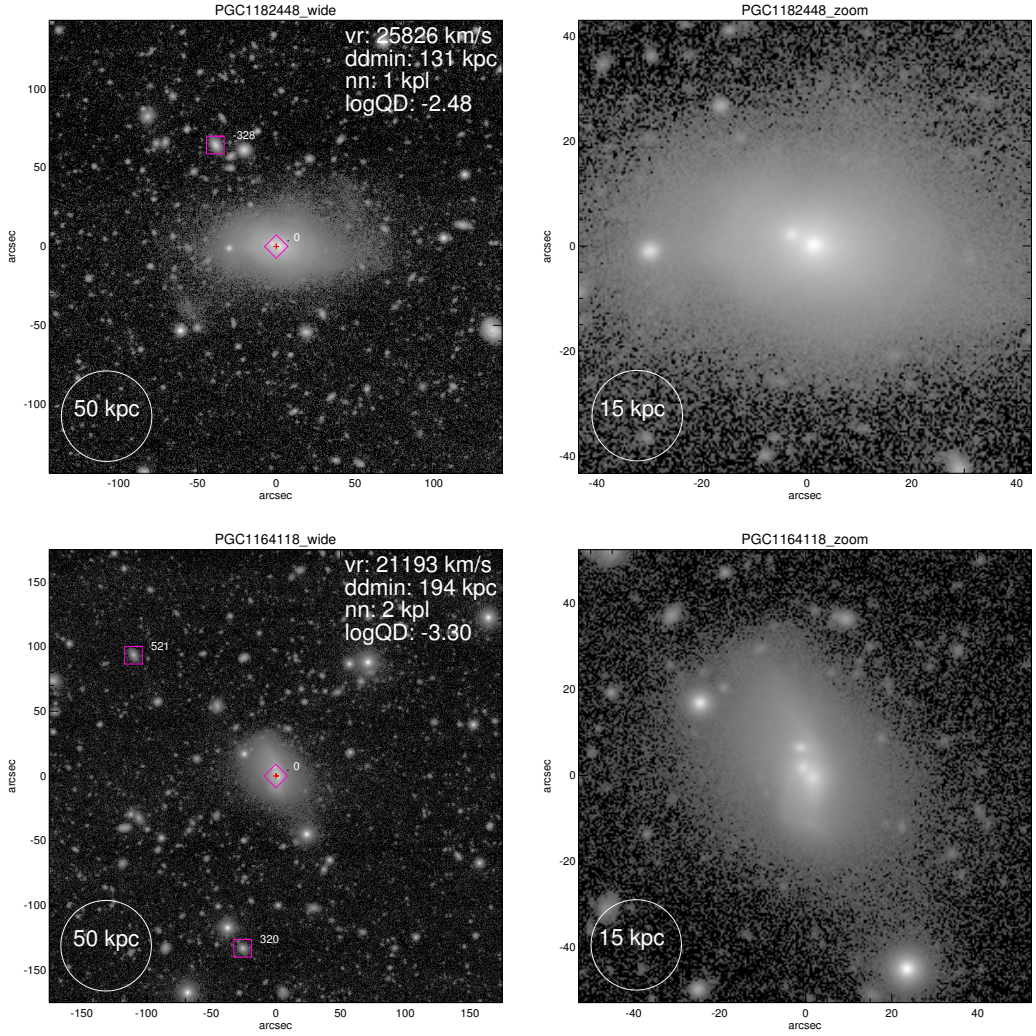

Figure 8: Two peculiar galaxies, PGC1182448 (upper row) and PGC1164118 (lower row). PGC1182448 has a shell structure, as well as a secondary nucleus, indicating a recent merger event. PGC1164118 has three nuclei, and odd three pronged structure around them, indicating a past merger of three galaxies. Both of these galaxies also have small nearby satellites, which are however insufficient in explaining the evident structures, and thus past merger events are implied.

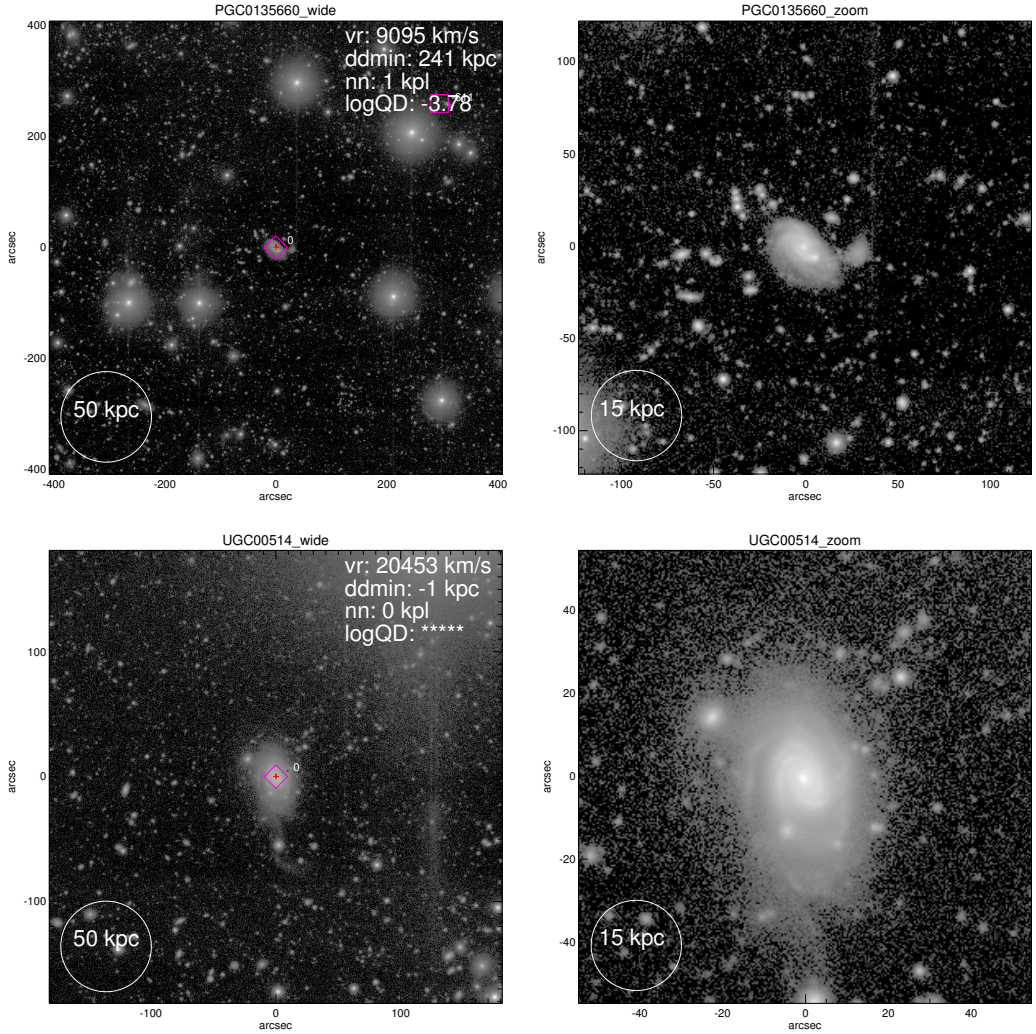

Figure 9: The exact borders between the different classes of interaction were difficult to define. I classified PGC0135660 (upper row) as a merger due to its two separate and equal nuclei, indicating a later stages of a merger. Classification as a peculiar could have worked as well however. UGC0051 (lower row) I classified as a peculiar because of its disturbed spiral structure as well as the odd tidal tail like structure protruding below it. Whether these structures could be formed in some other way than a recent merger is hard to say.

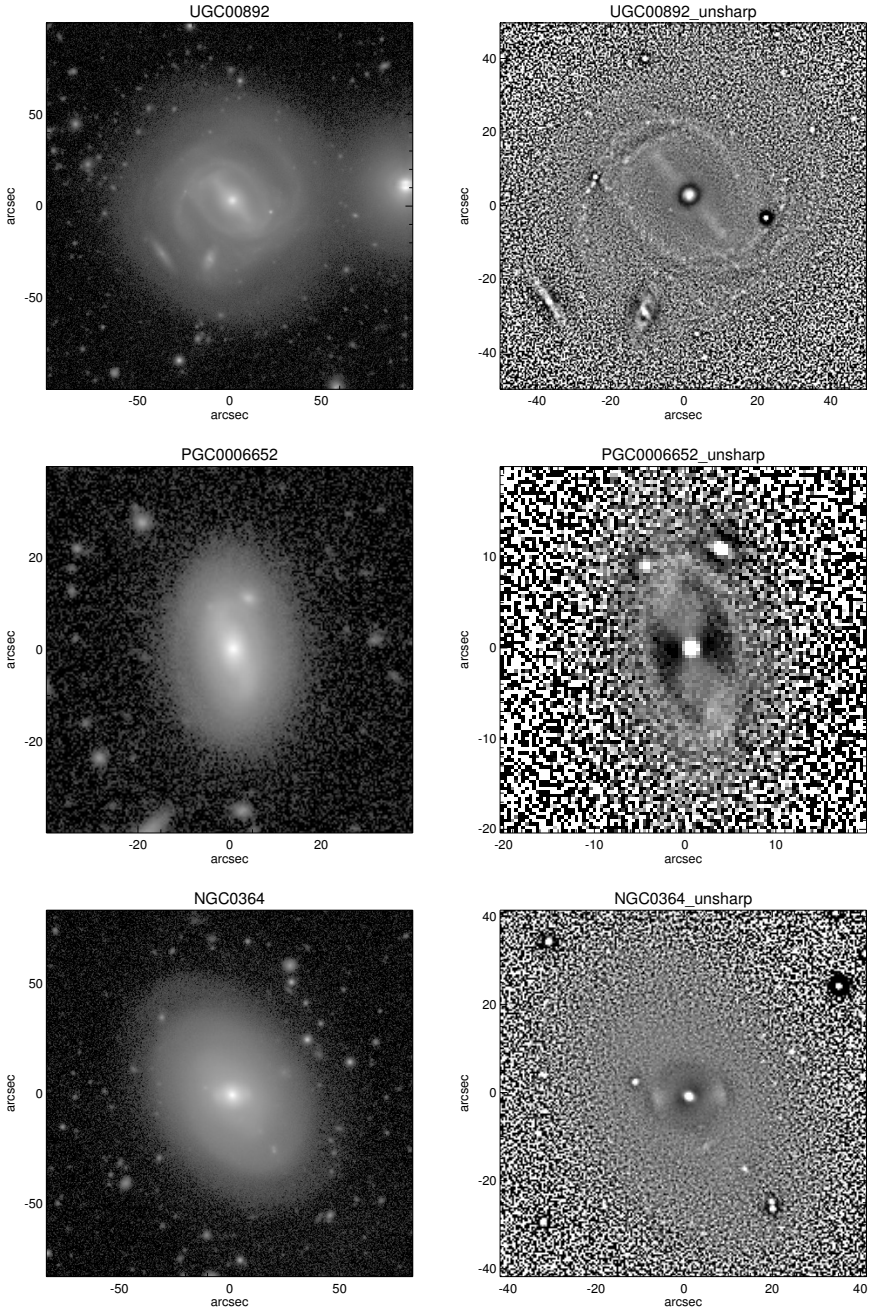

Figure 10: Barlens galaxies UGC00892 (upper row), PGC0006652 (middle row), and NGC0364 (bottom row). The left images are *i*-band images scaled to show a square with sides twice the D25 diameter of the galaxy, and the right ones are zoomed in unsharp masked versions with sides equal to the D25 diameter. PGC0006652 shows a X-shape in the unsharp mask. It was still classified as a barlens galaxy due to the barlens visible in the regular i-band image.

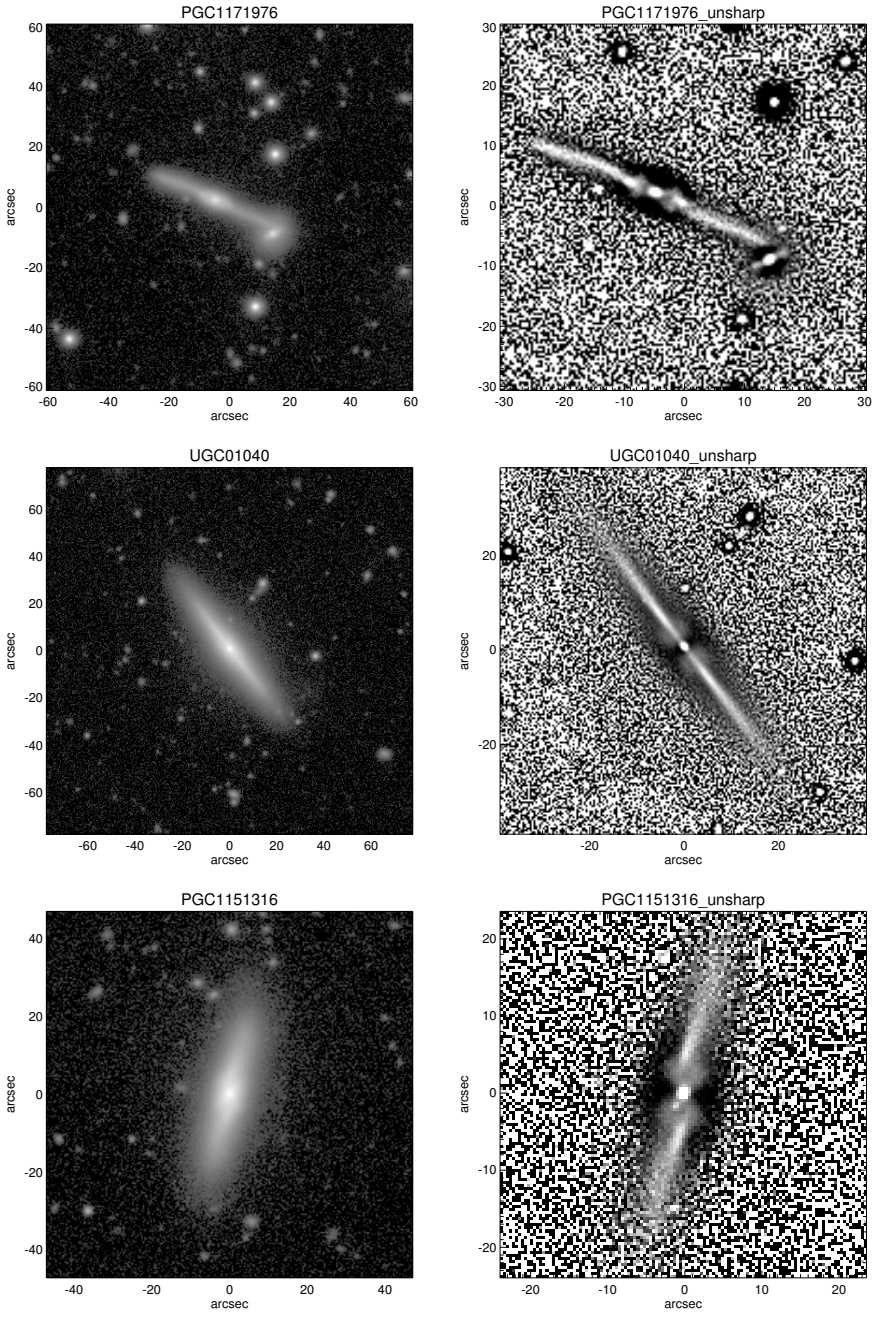

Figure 11: Clear X-shapes in galaxies PGC1171976 (upper row), UGC01040 (middle row), and PGC1151316 (bottom row).

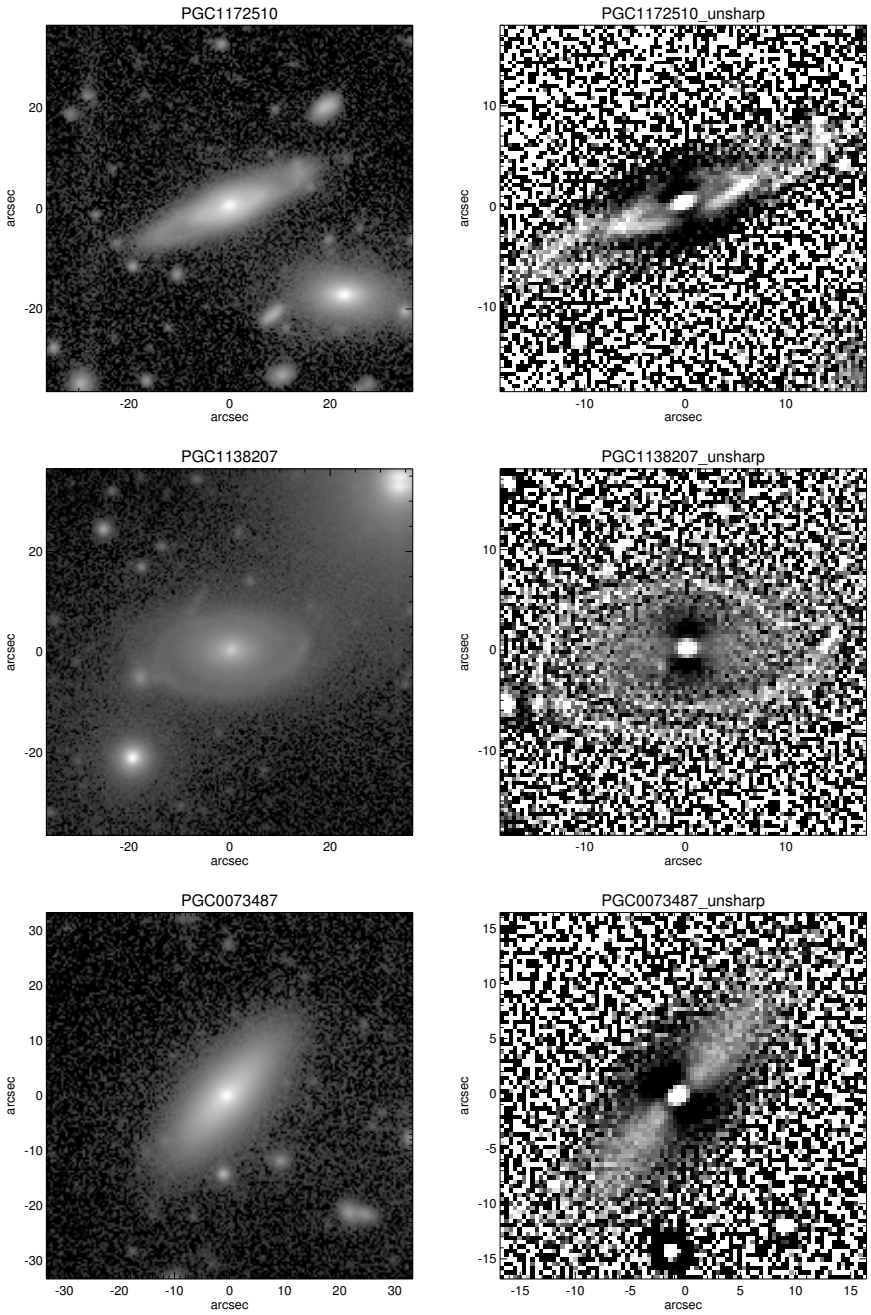

Figure 12: Unclear X-shapes in galaxies PGC1172510 (upper row), PGC1138207 (middle row), and PGC0073487 (bottom row). All of these galaxies are inclined rather than edge-on.

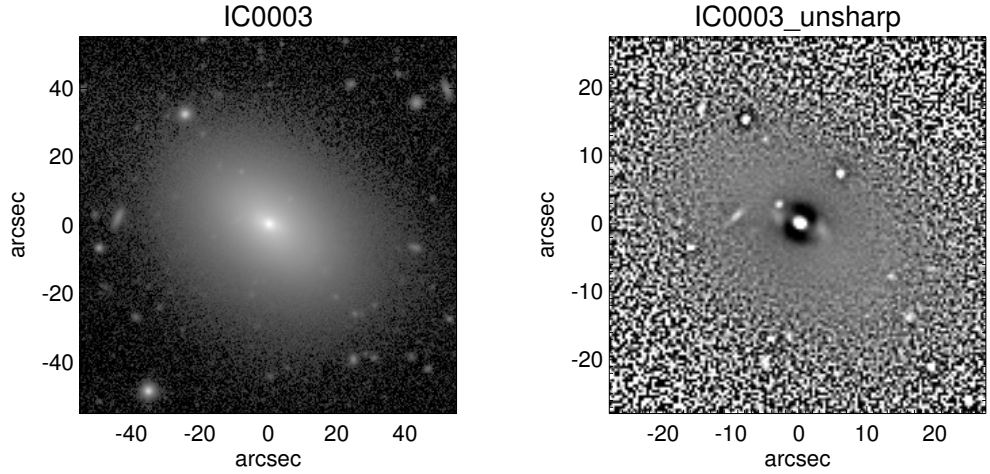

Figure 13: An example of an X-shape like structure visible in the unsharp mask of a seemingly elliptical galaxy IC0003. Classified as Hubble type E0 by Nair & Abraham (2010).

X-shapes'. Being found in elliptical galaxies, these are most likely not related to thick part of the bar, i.e. B/P bulges. These kind of boxy isophotes and X-shapes in ellipticals have been previously linked to galaxy interactions (Hernquist & Quinn, 1989). An example is shown in figure 13.

3 Results

3.1 Properties of the sample

Of the 1413 galaxies studied, total of 271 had experienced some sort of strong interaction: 210 of those were classified as interacting, 29 had an ongoing merger, and 32 were classified as peculiars. A barlens was identified in 49 galaxies, and 217 had an X-shape. Of the X-shapes 34 were classified as clear, and 183 as unclear. There were also 55 ellipticals with X-shape like structures visible in the unsharp masks. The numbers of different types of interaction and X-shape or barlens combinations are shown in table 1.

Most of the galaxies in the sample were spiral galaxies, with 900 galaxies of Hubble types Sa to Sm. 144 galaxies were elliptical and 271 lenticulars. The rest were irregular, unclassified or uncertain. There were more early type spiral galaxies than late types, with 727 galaxies of Hubble types Sa to Sc. The median absolute *i*-band magnitude was -21.1, very close to the value estimated for the

	No X/bl	Unclear X	Clear X	Barlens	Elliptical X
Non-interacting	876	157	29	39	41
Interacting	164	24	3	10	9
Merger	27	1	1	0	0
Peculiar	25	1	1	0	5

Table 1: The numbers of different types of interaction and B/P structure combinations in the sample.

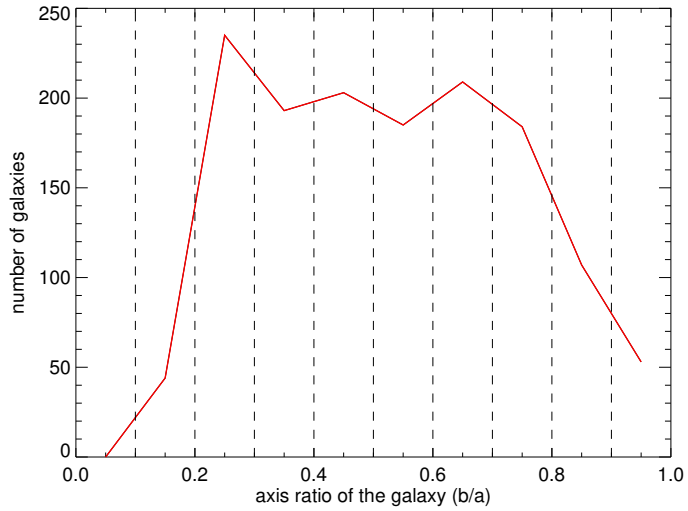

Figure 14: The minor-to-major axis ratio distribution of the whole sample in absolute scale. The sample is plotted in 0.1 axis ratio bins.

Milky Way ($M_{MW} = -21.3$; Licquia et al. 2015). The galaxies' axis ratio distribution was flat (figure 14) in the interval $b/a \approx 0.2 - 0.8$. The drop at zero is a natural consequence of the vertical thickness of the galaxies, but the drop close to $b/a \approx 1$ is more puzzling. A possible explanation is that HyperLEDA axial ratios are affected by the presence of non-circular internal isophotes, such as those of bars.

There were 472 barred galaxies in the sample, or about third of the galaxies. Of the barred galaxies 147, or 31% had a barlens or an X-shape. Of the 941 galaxies classified as unbarred in HyperLEDA, 123 had a barlens, a clear X-shape or an unclear X-shape.

Both the clear and unclear X-shapes had a similar relation to interaction, and I found no significant differences in their distributions in regards to any of the parameters studied. I consider them as single species in the following to achieve better statistics. I suspect that the differences between the appearances of the clear

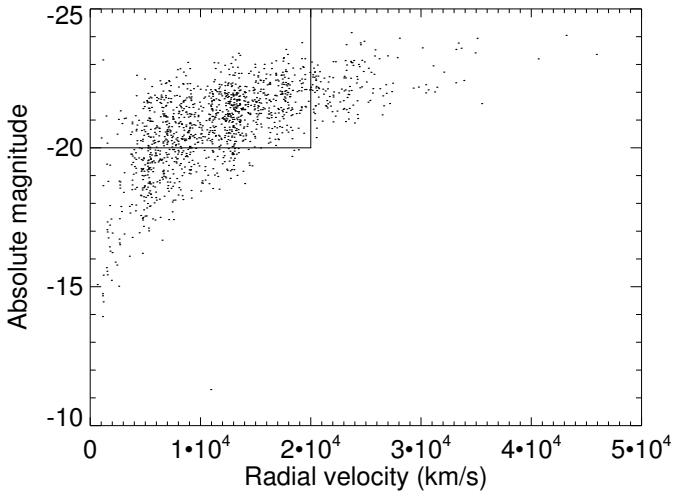

Figure 15: Radial velocity distribution of the galaxies of my sample versus their absolute *i*-band magnitude. The more complete subsample of 915 galaxies is shown as the boxed off area at top left.

and unclear X-shapes come mostly from image quality, inclination, and obscuring galactic features such as dust lanes.

A sample selected by apparent size is not a complete sample, as can be seen from figures 15 and 16, since at large distances only bright galaxies are seen. To investigate any errors produced by the incompleteness I also performed the statistical analysis with a nearly complete subsample of 915 galaxies. The subsample was taken by limiting the absolute *i*-band magnitude to $M_{abs} < -20$ and radial velocity to $v_r < 20000$ km/s. The only significant differences between the full sample and the subsample was that the subsample had a slightly higher fraction of barlenses and X-shapes among both interacting and non-interacting galaxies. This is expected as the subsample is limited to large, well-defined galaxies. In the following I present the statistical analysis for the whole sample, as it gave rise to smoother plots.

3.2 X-shapes and barlenses in interacting and non-interacting galaxies

There were enough interacting galaxies with X-shapes and barlenses for fairly good statistics: 27 galaxies were interacting and had X-shapes, while 10 galaxies were interacting and had barlenses (table 1). Figure 17 shows two examples of interacting galaxies with X-shapes, while figure 18 shows two interacting barlens

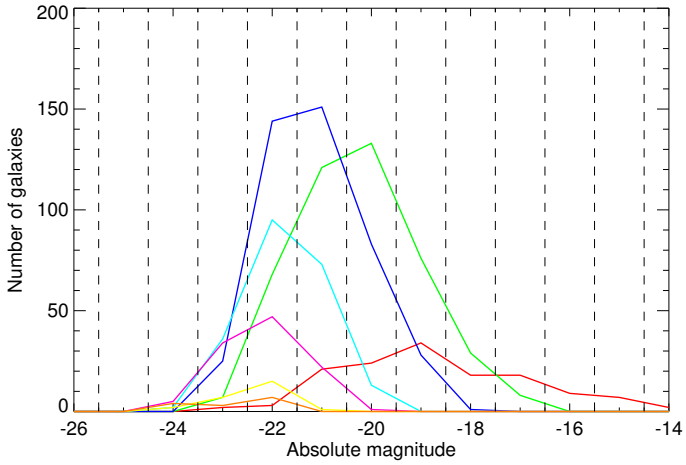

Figure 16: The absolute *i*-band magnitude distributions of different radial velocity bins. Red line is for 0 to 5000, green for 5000 to 10000, dark blue for 10000 to 15000, light blue for 15000 to 20000, purple for 20000 to 25000, yellow for 25000 to 30000 and orange for 30000 to 35000 km/s. Larger radial velocities (distances) have the peak distribution at brighter absolute magnitudes.

galaxies.

In non-interacting galaxies, 16.3% $\pm$ 2.2% [2] had X-shapes, while only 12.9% $\pm$ 4.6% of interacting galaxies had them. In the near complete subsample, the fractions of X-shapes were 18.6% $\pm$ 2.9% for non-interacting galaxies, and 15.4% $\pm$ 5.9% for interacting ones.

A total of 3.4% $\pm$ 1.1% of the non-interacting galaxies had barlenses, while 4.8% $\pm$ 2.9% of the interacting ones had them. In the subsample, 4.8% $\pm$ 1.6% of the non-interacting and 6.0% $\pm$ 3.9% of the interacting galaxies had barlenses. Interestingly this would seem to suggest that interaction would destroy X-shapes but create barlenses. However, judging from the 2σ error bars, the differences are not statistically significant. These fractions are also presented in table 2 for convenience.

3.2.1 Dependence on inclinations

Figure 19 shows a density plot of the absolute *i*-band magnitude distribution of the galaxies versus their inclination, with barlenses and X-shapes marked. At first glance a number of observations can be made from the figure:

[2] All the errors in this study are given with a 95%, or 2σ confidence level. They are calculated using the normal distribution approximation as $\pm 1.96\sqrt{p(1-p)/n}$, where p is the fraction and n is the total number of galaxies in the category.

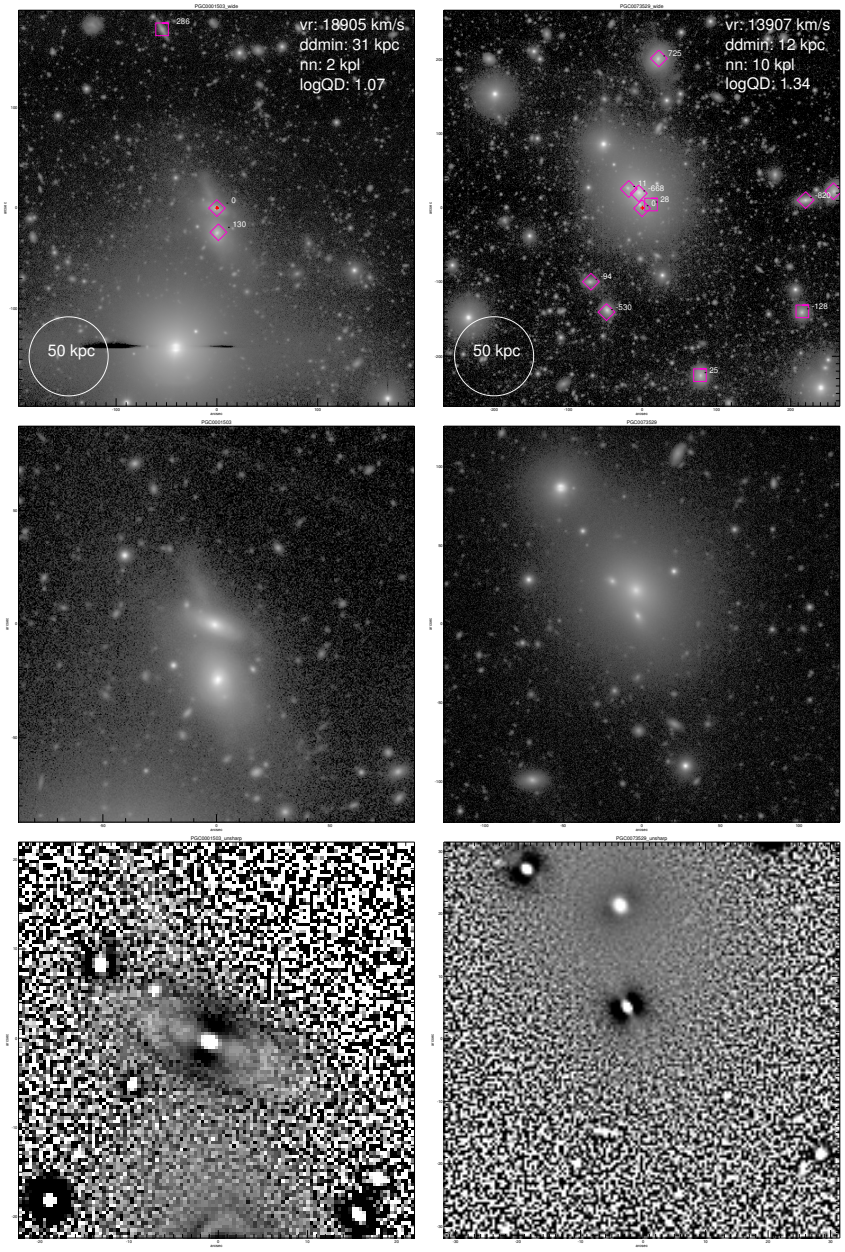

Figure 17: Interacting galaxies with X-shapes PGC0001503 (left) and PGC0073529 (right). The top row is in the 'ultra-deep *r*-band', while the middle row is in *i*-band and the bottom row is an unsharp mask of the *i*-band.

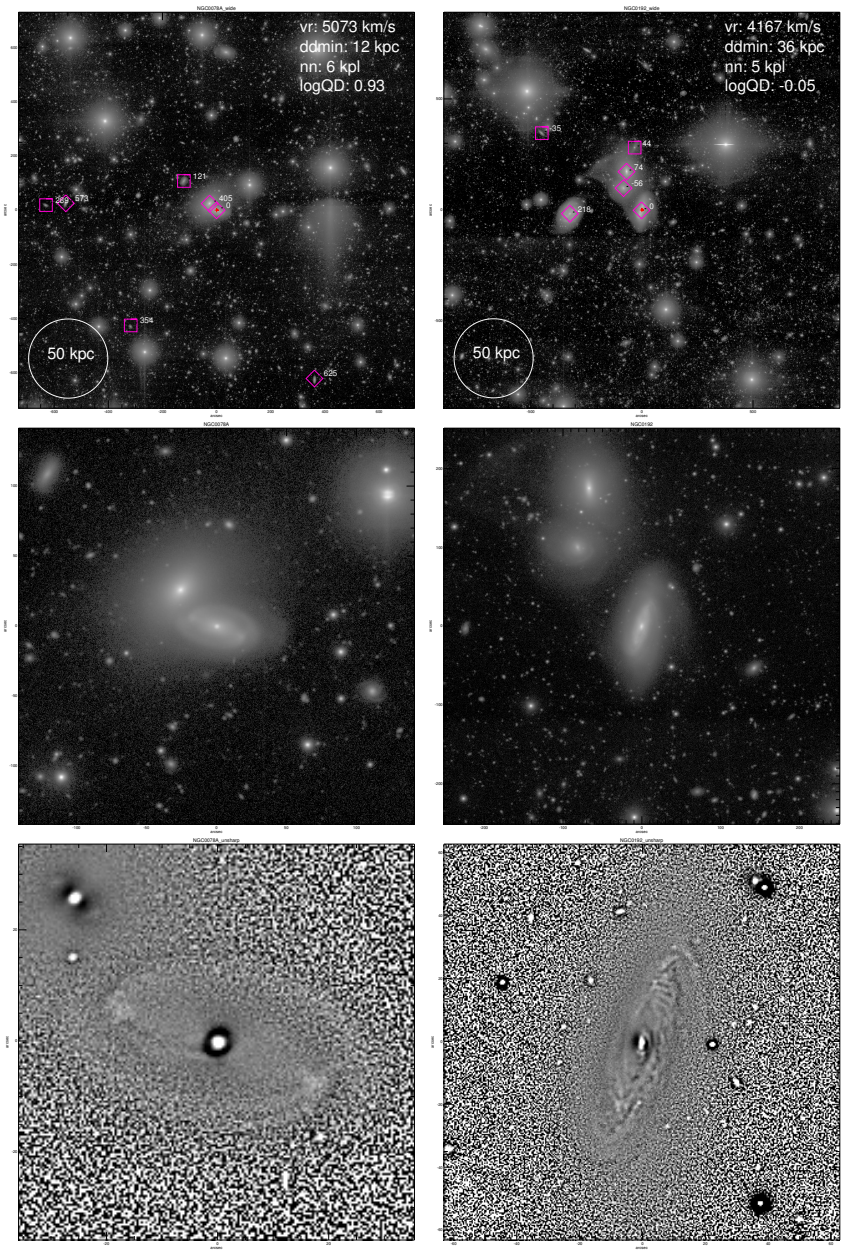

Figure 18: Interacting galaxies with barlenses NGC0078A (left) and NGC0192 (right). NGC0078A is a part of a pair of galaxies while NGC0192 is part of a tight group of six galaxies.

	Full sample		
	No X/bl	X-shape	Barlens
Non-interacting	$76.7\% \pm 2.5\%$	$16.3\% \pm 2.2\%$	$3.4\% \pm 1.1\%$
Interacting	$78.1\% \pm 5.6\%$	$12.9\% \pm 4.6\%$	$4.8\% \pm 2.9\%$
	Subsample		
	No X/bl	X-shape	Barlens
Non-interacting	$72.0\% \pm 3.3\%$	$18.6\% \pm 2.9\%$	$4.8\% \pm 1.6\%$
Interacting	$73.8\% \pm 7.1\%$	$15.4\% \pm 5.9\%$	$6.0\% \pm 3.9\%$

Table 2: The main central feature fractions in interacting and non-interacting galaxies for the full sample as well as for the more complete subsample.

- As expected, X-shapes are much more common in highly inclined galaxies, while barlenses are more common in lower inclinations.
- There is no clear difference in the distribution of interacting galaxies compared to the distribution of all galaxies.
- The sample is biased towards low absolute magnitudes and high inclinations. This is most likely a selection bias towards a higher surface brightness.
- There is no clear difference in the distribution of X-shapes and barlenses between interacting and non-interacting galaxies.

Looking in more detail the inclination distributions of X-shapes and barlenses (Figure 20), there is a hint that in higher inclinations, the interacting galaxies appear to have less X-shapes compared to the non-interacting galaxies. In low inclination galaxies the opposite appears true, interacting galaxies have more X-shapes than non-interacting galaxies. However, this trend is not statistically significant, as can be seen from the error bars.

In barlenses the only potential difference between interacting and non-interacting galaxies is that there seems to be a slight excess of very high inclination, basically edge-on barlens galaxies among the interacting galaxies.

When considering the X-shapes and barlenses as single species, as in figure 21, the differences between interacting and non-interacting galaxies are reduced and the distribution becomes flatter. A significant excess of boxy features is still left in the high inclination galaxies.

3.2.2 Dependence on absolute galaxy magnitudes

From the absolute *i*-band magnitude distribution in figure 22 we can see that barlenses are more common in brighter galaxies. X-shapes share the same trend, but

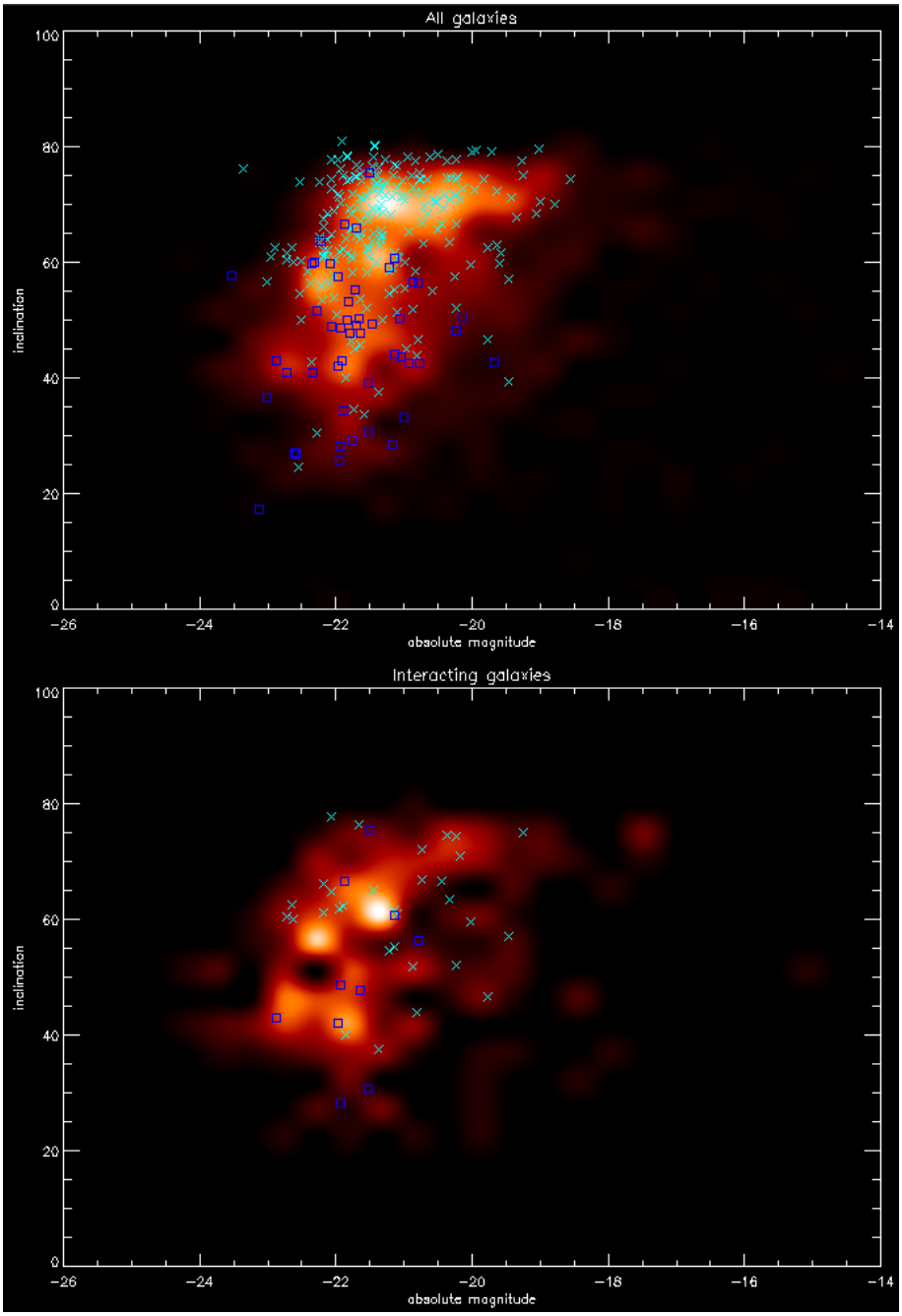

Figure 19: The absolute *i*-band magnitude—inclination density plot of the sample. Hotter color means higher number of galaxies per bin. X-shapes are marked as light blue 'x' and barlenses as dark blue boxes. The upper plot shows all the galaxies and the lower one only the interacting ones.

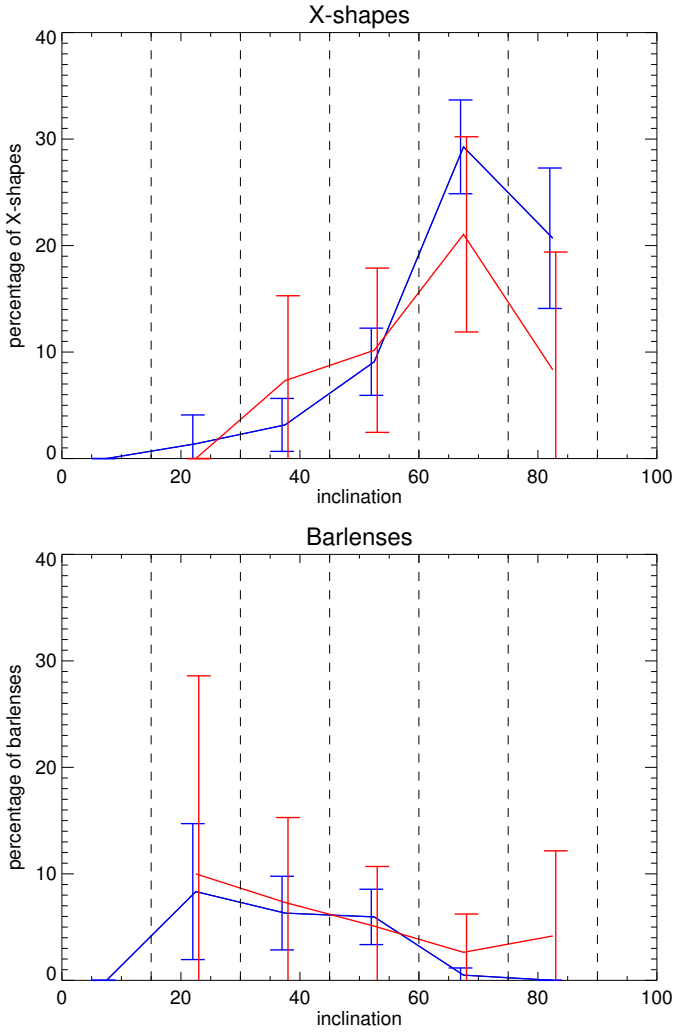

Figure 20: The dependence of the fraction of X-shapes and barlenses on inclination. The upper plot shows the fraction of X-shapes in blue for non-interacting galaxies and in red for interacting galaxies. The lower plot shows the same for barlenses. The sample is plotted in 15° inclination bins. The error bars in all the figures of this study are given with a 95%, or 2σ confidence level.

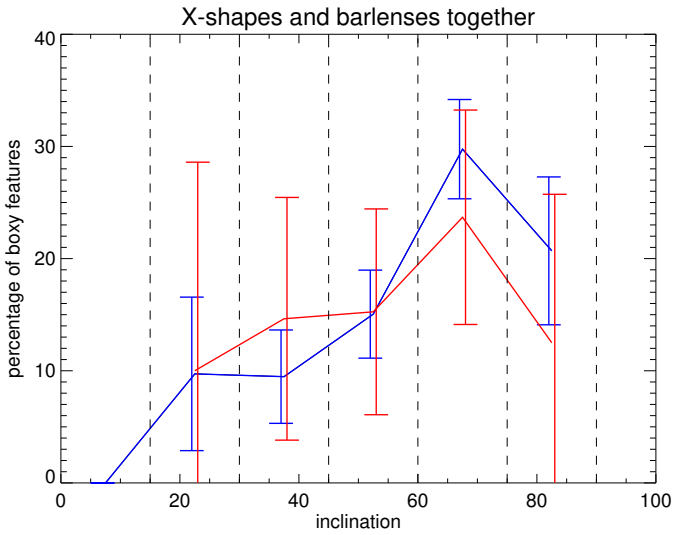

Figure 21: The dependence of the fraction of galaxies with either X-shape or barlens on inclination. Blue is for non-interacting and red for interacting galaxies.

not necessarily in interacting galaxies. We can also see that in bright galaxies there is a statistically significant difference between interacting and non-interacting galaxies in regards to X-shapes. In galaxies of absolute *i*-band magnitude (M_{abs}) of about -22, among interacting galaxies there is less than half of the amount of X-shapes compared to non-interacting galaxies, and the difference is much larger than the 2σ error bars. The statistics is especially robust here, as in the sample there are 288 non-interacting galaxies and 68 interacting galaxies in the range $-22.5 < M_{abs} < -21.5$.

If we restrict only to galaxies of high inclinations ($> 60°$), the galaxies where X-shapes are expected, the trend of interacting galaxies having less X-shapes extends to $M_{abs} \sim -21$ as well. This can be seen in figure 23.

As complex structures are much more common in larger galaxies, and X-shapes are traditionally found in high inclination galaxies, this result is actually quite general. By just taking Milky Way luminosity and brighter ($M_{abs} < -21$) high inclination ($i > 60°$) galaxies, we find that nearly half ($47.4\% \pm 6.8\%$) of non-interacting galaxies have X-shapes, while only around fifth ($20.0\% \pm 11.1\%$) of interacting galaxies have them. As galaxy's luminosity is primarily dependent on its stellar mass, this can be thought of as a property of massive galaxies.

In addition, this trend seems to be reversed in lower luminosity galaxies of $M_{abs} > -20$, with interacting galaxies having more X-shapes. However, this is statistically insignificant due to the low amount of interacting galaxies of those magnitudes.

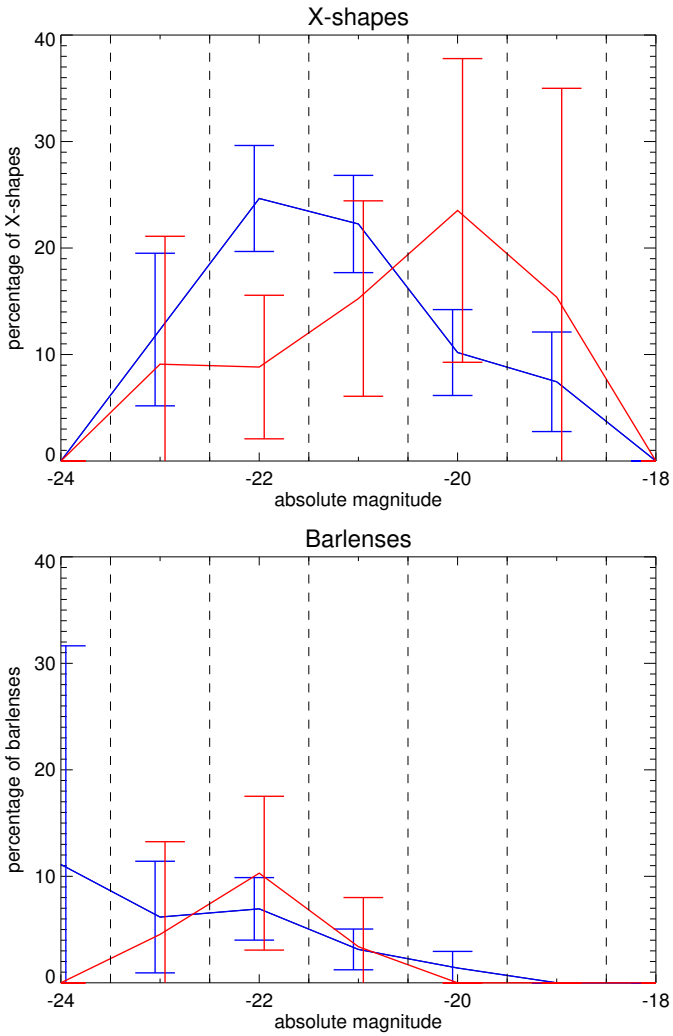

Figure 22: The dependence of the fraction of X-shapes and barlenses on absolute *i*-band magnitude. The upper plot shows the fraction of X-shapes in blue for non-interacting galaxies and in red for interacting galaxies. The lower plot shows the same for barlenses. For X-shapes the difference between interacting and non-interacting galaxies is notable for galaxies of $M_{abs} \sim -22$, with X-shapes being more than twice as common in non-interacting galaxies. The sample is plotted in one magnitude bins.

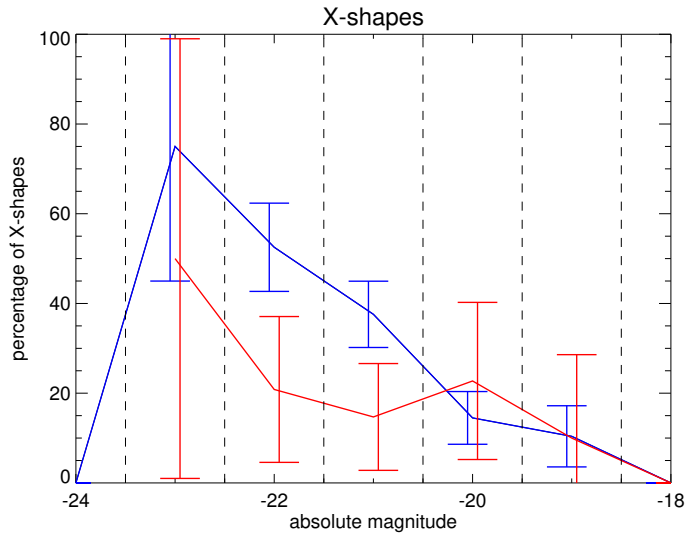

Figure 23: The dependence of the frequency of X-shapes on absolute magnitude for galaxies of above $60°$ inclination. The statistically significant difference between interacting and non-interacting galaxies extends down to $M_{abs} \sim -21$.

With barlenses there does not seem to be any significant difference in the frequency of them versus absolute magnitude, when interacting and non-interacting galaxies are compared.

3.2.3 Dependence on Hubble types

The dependence of the occurrence of X-shapes and barlenses on morphological types is shown in figure 24. Both the X-shapes and barlenses seem to be concentrated on early type spiral galaxies, the X-shapes even more heavily. Barlenses have a peak at Hubble types $T = +1$ and $T = +2$, while X-shapes are equally as common also among types $T = 0$ and $T = -1$. There is a dip in the distribution of X-shapes in interacting galaxies at $T = +1$ and $T = +2$ compared to non-interacting galaxies, but as can be seen from the error bars, it is not statistically significant.

3.2.4 Bar fractions

The bar fraction dependence on galaxy inclination, absolute *i*-band magnitude and morphological type is shown in figure 25. The bar data for these plots is from HyperLEDA. As B/P bulges are heavily related to bars, comparison between the bar and X/bl distributions is interesting.

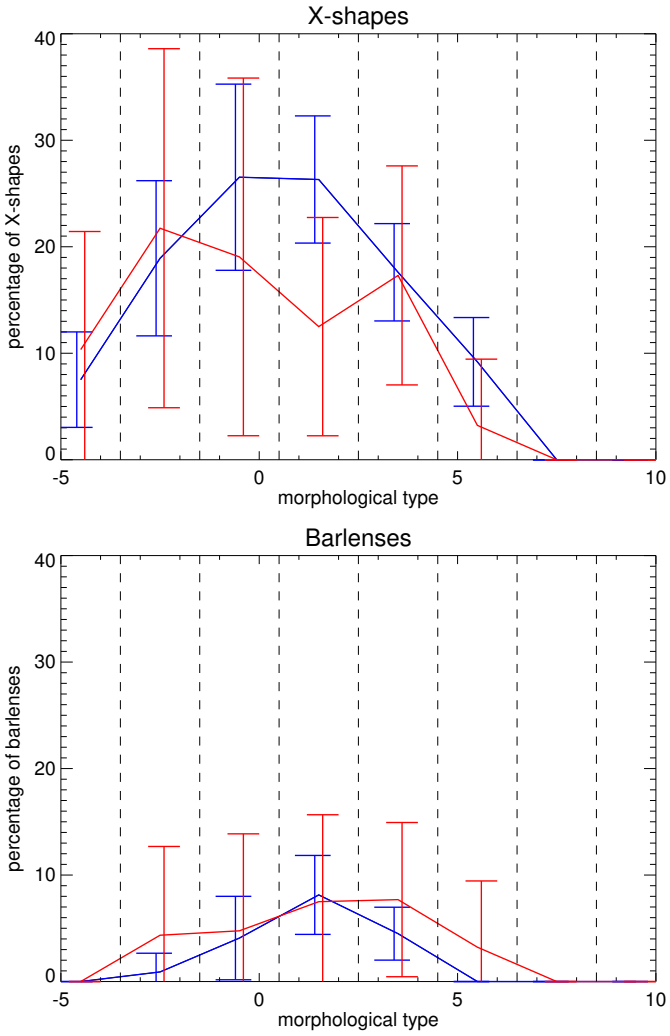

Figure 24: The dependence of the fraction of X-shapes and barlenses on morphological type. The upper plot shows the fraction of X-shapes in blue for non-interacting galaxies and in red for interacting galaxies. The lower plot shows the same for barlenses. The morphological types have been assigned the common numerical codes, with -5 being elliptical galaxies (E), -3 to 0 the lenticular galaxies (S0) and 1 to 9 the spiral galaxies (Sa to Sm). The sample is plotted in bins encompassing galaxies from two adjacent type codes. The morphological type data is from HyperLEDA.

For inclinations, the bar fraction distribution is flat as it should be, meaning that there is no inclination bias in HyperLEDA bar data. There appears to be no difference between interacting and non-interacting galaxies.

The bars seem to be concentrated on less bright galaxies than X/bl features, the bar fraction staying flat for even the faint $M_{abs} > -18$ galaxies, compared to the X/bl fractions which dropped to zero at $M_{abs} = -18$. There is no difference between interacting and non-interacting galaxies, except for the statistically insignificant noise below $M_{abs} > -20$.

In the Hubble type distribution bars are concentrated on later types than the X/bl features, with the bar distribution going flat for spiral galaxies ($+1 < T < +9$). Again there seems to be no difference between the interacting and non-interacting galaxies, except perhaps for very late type galaxies ($+7 < T < +10$) for which there is only poor statistics.

3.3 X-shapes in mergers and peculiars

Two of the galaxies classified as mergers had X-shapes, as well as two of the peculiars. No merger or peculiar galaxy had a barlens. As such, any statistics derived from these are fairly shaky, and they are treated here as a single group. All of these galaxies are shown in figure 26.

Overall there seems to be fewer X-shapes among mergers and peculiars than among non-interacting galaxies. And as figure 27 demonstrates, this difference seems to be even statistically significant among galaxies of high inclinations and bright luminosities. These results are similar to those derived for the interacting galaxies. The only significant difference to the interacting galaxies seems to be a potential absence of X-shapes in fainter galaxies. However, this is most likely explained by the small number of mergers and peculiars in the sample. It must be noted that the error bars were calculated with the normal distribution approximation, which loses reliability at small sample sizes. Additionally, if we take the nearly complete subsample, of which all four galaxies are part of, all significant differences between the distributions of the merger/peculiar galaxies and the non-interacting galaxies vanish.

4 Discussion

4.1 Differences between interacting and non-interacting galaxies.

I performed the chi-square contingency table test (Wall & Jenkins, 2003), to see whether or not the occurrence of different central structures (X, bl, no X/bl) could

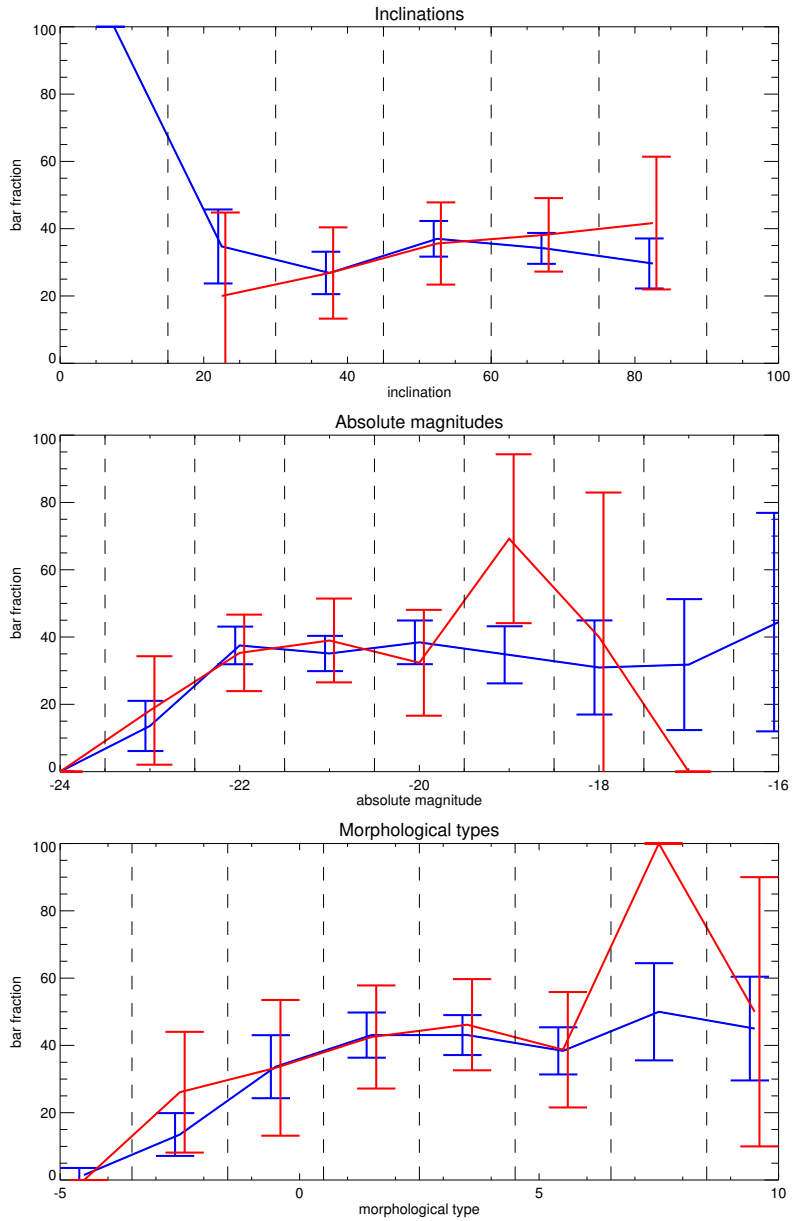

Figure 25: The dependence of the bar fraction on inclination, absolute magnitude and morphological type. The blue lines are for the non-interacting galaxies and the red lines for the interacting ones. The upper plots shows the dependence on inclination, the middle plot shows the dependence on absolute magnitude, and the lower plot the dependence on morphological type. The bin sizes are the same as for X/bl features. The 100% peaks are caused by cases of bins with less than five galaxies all happening to have bars.

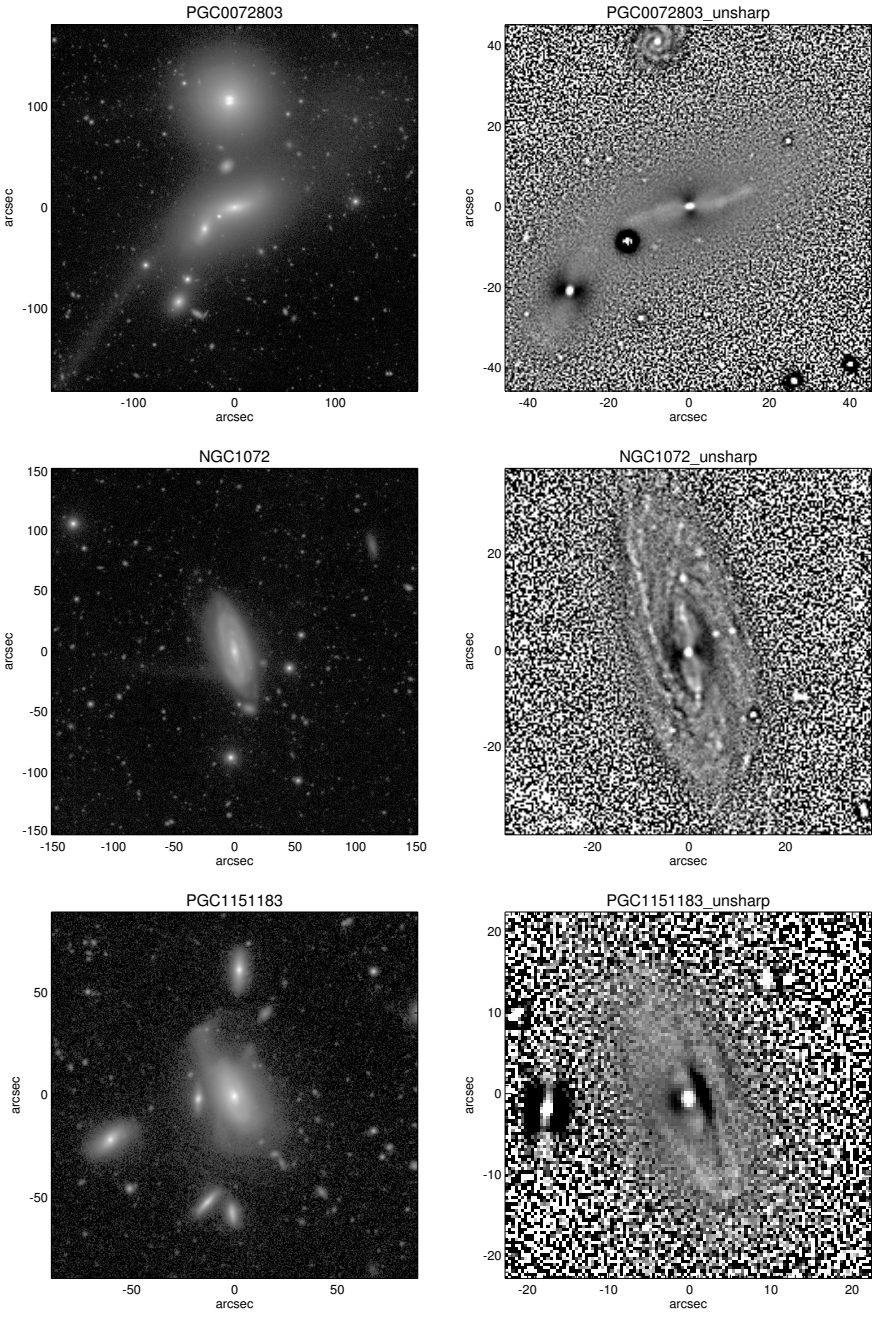

Figure 26: All of the mergers and peculiars with X-shapes. Top row: merger pair PGC0072803 and PGC0072808. The image is centered on PGC0072803, while PGC0072808 is visible on the bottom left corner of the unsharp mask. Middle row: peculiar NGC1072. Bottom row: peculiar PGC1151183. The left images are in *i*-band, and the right ones are the unsharp masks of them.

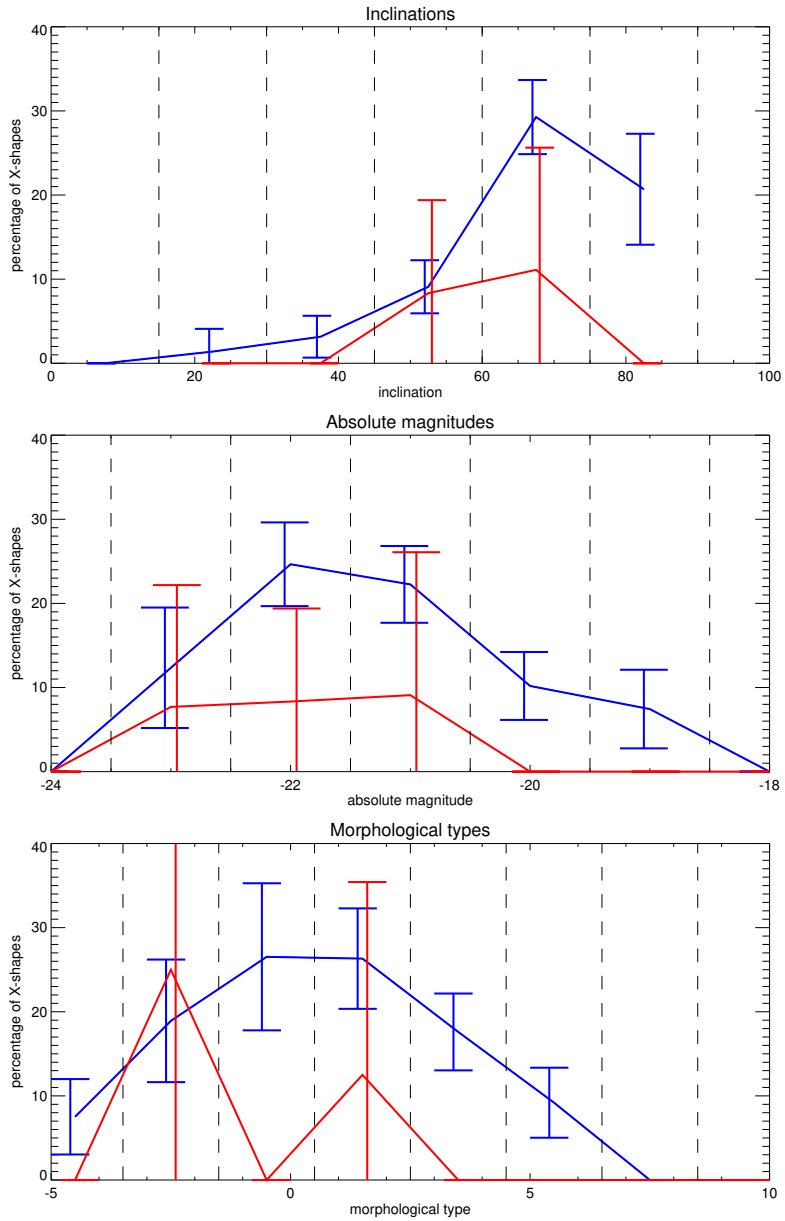

Figure 27: The dependence of the fraction of X-shapes on inclination, absolute magnitude and morphological type for mergers and peculiars. On blue is shown the fraction for non-interacting galaxies and on red for mergers and peculiars. The upper plot shows the dependence on galaxy inclination, the middle on absolute *i*-band magnitude and the lower on morphological type. Similar fraction drop of X-shapes for merger and peculiar galaxies of $M_{abs} \sim -22$ is apparent as for interacting galaxies.

	No X/bl	X-shape	Barlens
Non-interacting	876	186	36
Interacting	164	27	10

Table 3: The contingency table used for the chi-square tests.

be considered as independent of the galaxy being interacting or not. The null hypothesis (H_0) is that the fact whether a galaxy is interacting or not, has no effect on the occurrence of these central structures (X, bl, no X/bl). The chi-square value is given by equation 5, where O_{ij} are the values of the contingency table, the sums are over columns (k) and rows (r), and E_{ij} are given by equation 6. Due to the limitations of the chi-square test (no bin should have less than 5 objects) I combined the two X-shape categories (clear and unclear) and disregarded mergers, peculiars and elliptical X-shapes in this test. The contingency table is shown in table 3. The sampling distribution of χ^2 when H_0 is valid, follows chi-square distribution with 2 degrees of freedom in a case of 3 x 2 contingency table (given by equation 7). The test gave $\chi^2 = 2.72$, which for $\nu = 2$ has a probability of 25.6% , meaning that H_0 is not rejected.

$$\chi^2 = \sum_{i=1}^{r}\sum_{j=1}^{k}\frac{(O_{ij} - E_{ij})^2}{E_{ij}} \tag{5}$$

$$E_{ij} = \frac{\sum_{j=1}^{k} O_{ij} \sum_{i=1}^{r} O_{ij}}{\sum_{i=1}^{r}\sum_{j=1}^{k} O_{ij}} \tag{6}$$

$$\nu = (r-1)(k-1) \tag{7}$$

I also performed the modified 2 x 2 chi-square test with only the galaxies with X-shapes or barlenses, to see whether they could be considered as single species in regards to their relation to galaxy interactions. The H_0 means that the occurrences of X-shapes and barlenses are independent of galaxy interaction. The chi-square for the 2 x 2 table is given by equation 8, where A, B, C, and D are the values of the table and N is the total number of objects. The contingency table used was table 3 without the 'No X/bl' column. This gave $\chi^2 = 2.54$, which for a 2 x 2 table with $\nu = 1$ has the probability 11.1%, so H_0 is not to be rejected.

$$\chi^2 = \frac{N(|AD - BC| - N/2)^2}{(A+B)(C+D)(A+C)(B+D)} \tag{8}$$

As the chi-square tests reveal, the statistics of my sample are not robust enough to make any definitive statements about the differences of barlens and X-shape occurrences in interacting and non-interacting galaxies. As such, the apparent

differences between barlens and X-shape distributions in regards to interaction (table 2) are not significant. Even if the different relations to interactions would be found significant with better statistics, it would not contradict the idea that barlenses and X-shapes are both visual projections of a single physical entity. The face-on seen barlenses are the disc plane projection of the bar related feature called B/P bulge, while the edge-on seen X-shapes are its vertical projection. The different projections of the complicated three dimensional B/P structure could be affected by tidal forces in a such way that makes more difficult the detection of X-shapes while making the detection of barlenses easier.

There were slight differences in the inclination distributions of the interacting and non-interacting X-shape galaxies (figure 20). Namely, interacting high inclination galaxies seemed to have less X-shapes than non-interacting ones, while no such a trend, or even an opposite trend, was visible for the low inclination galaxies. While the differences were well within the 2σ confidence level margins of errors, they are still interesting to note, as they seem to hint that low inclination X-shapes react similarly to interaction as barlenses. This would suggests that the vertical (normal to the disc plane) edge-on structure of B/P bulges may be more sensitive to interaction than the disc plane face-on structure.

One way that the vertical and disc plane features could be decoupled is if interaction destroys the bar of the galaxy. As the X-shape is maintained by the vertical resonances of the bar, the destruction of the bar would also cause the disappearance of the X-shape structure. Planar central concentration such as the circular part of a barlens could however survive this event. The problem with applying this process to my results it that the surviving structure would not readily look like a barlens (thin bar component absent), and would more likely be identified as a classical bulge or discy pseudobulge, and as such the destruction of the bar would also cause a reduction in the number of barlenses detected. Additionally, in my sample the interactions did not seem to affect the bar fraction noticeably, with 33% of the non-interacting galaxies hosting bars, compared to the 35% of the interacting galaxies, and 28% of the mergers and peculiars, all within each others uncertainties.

4.1.1 X-shapes of massive galaxies

The most statistically significant difference between the interacting and non-interacting galaxies was the reduction of the fraction of X-shapes in bright (massive) interacting galaxies (see figures 22 and 23 and section 3.2.2). X-shapes are present in only fifth of the massive, high-inclination interacting galaxies compared to the nearly half the of non-interacting ones. This reduction is most significant in the peak of the X-shape absolute *i*-band magnitude distribution of the non-interacting galaxies, at $M_{abs} \sim -22$, but can be generalized to all massive high inclination

galaxies. Figure 28 shows examples of the $M_{abs} \sim -22$ galaxies with X-shapes.

This seems to suggest that while X-shapes are more common in more massive galaxies, they are also less stable and more susceptible to disturbance by interactions. Massive galaxies could be more favorable platforms for X-shape formation, but also for X-shape destruction. This idea is somewhat supported by Li et al. (2017), who found that buckled bars (B/P/X/bl structures) are more common in more massive galaxies. They also found more buckled bars among early type disc galaxies, while bars in general were common also in late types and less massive galaxies, matching well with my observations. Another parameter they found that affected the fraction of buckled bars was the gas fraction, with the buckled bar fraction going down as gas mass fraction went up. Interactions are well known to affect star formation rates, which in turn are dependent on the gas fractions. A recent study by Pan et al. (2018) suggests that it is indeed the gas fraction that goes up in interactions, rather than the efficiency of star formation. The reduction of X-shape fraction I observed may be related to tidal interactions affecting the gas properties of the host galaxies.

As face-on projections of the same structures, one would expect this reduction to be visible on the barlens fraction as well. However, this is not the case. This may be caused by the smaller number of barlenses found, or it could again hint of a higher durability of the disc plane structure.

4.1.2 Strong interaction versus weak interaction

It is obvious that very strong interactions between galaxies, such as mergers, should destroy any rotationally supported structures, like B/P bulges. As expected, there were proportionally less X-shapes and barlenses found among the merger and peculiar galaxies, and in fact no barlenses were found among them. It is still interesting to note that any X-shapes at all were found among the relatively few merger and peculiar galaxies of the sample, which speaks of the potential robustness of these structures.

Of the four X-shape galaxies classified as mergers or peculiars (figure 26), the two merging galaxies, PGC0072803 and PGC0072808, were still in the relatively early phases of the merging process, allowing the survival of the X-shapes. The reason why NGC1072 was classified as a peculiar galaxy was the strange tail protruding from the lower left of the galaxy. It is hard to say what kind of interaction might have caused it. Whatever the case, the X-shape survived.

PGC1151183 is perhaps the most interesting one of the four. It has two smaller nearby companions, as can be seen from figure 29, but it is unlikely that the heavy distortion in the main galaxy could be caused by the two companions alone. The galaxy has most likely undergone a recent major merger, which means that either the X-shape of one of the galaxies must have somehow survived the event, or a

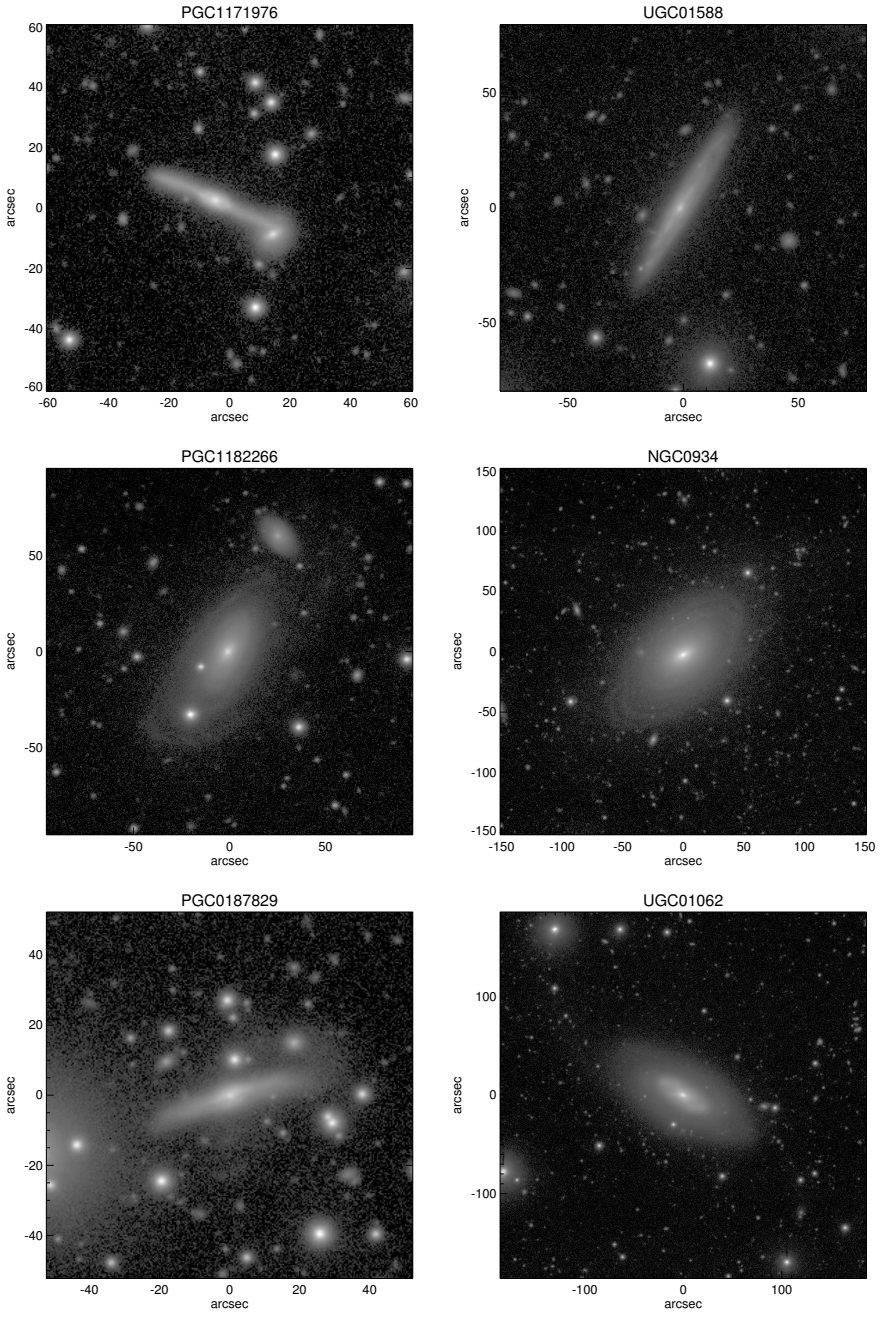

Figure 28: X-shape hosting galaxies with $-22.5 < M_{abs} < -21.5$ in *i*-band. PGC1171976, PGC1182266 and PGC0187829 on the left are interacting, while UGC01588, NGC0934 and UGC01062 on the right are non-interacting. All of them have X-shapes, PGC1171976 and UGC01588 clear ones and the rest unclear ones. Images are in *i*-band.

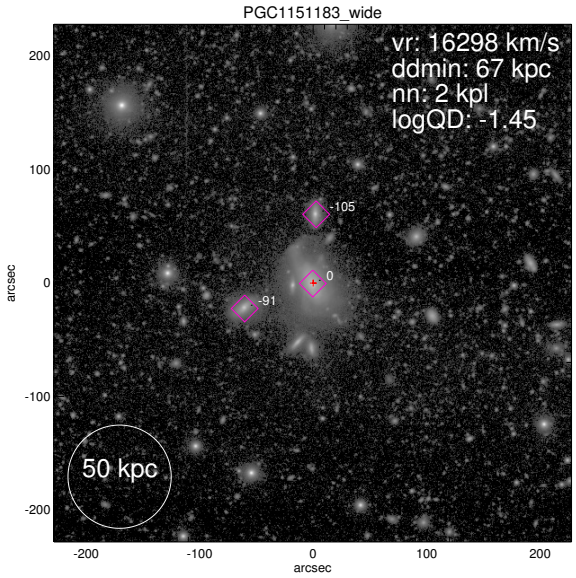

Figure 29: PGC1151183 and its companions. Image is in the 'ultra-deep *r*-band'.

new one has developed exceptionally quickly. Either way it is remarkable that a B/P structure can exist in such a violent environment.

It must be noted that while there were no barlenses among mergers and peculiars, this is most likely caused by just the incompleteness of the sample. There were over four times as many X-shapes than barlenses among the whole sample, and only four X-shapes among the mergers and peculiars.

4.2 Quality of the data

4.2.1 Comparison to earlier work

One way to measure the validity of these results is to compare them to those of earlier studies. Laurikainen et al. (2014) used Spitzer Survey of Stellar Structure (S^4G; Sheth et al. 2010) and Near-IR S0-Sa galaxy Survey (NIRS0S; Laurikainen et al. 2011) for a total sample of 2465 nearby galaxies, from which they used a magnitude limited subsample of 597 galaxies for their statistical analysis. Their subsample contained 61 barlenses (10.2%) and 42 X-shapes (7.0%), meaning their sample had proportionally less X-shapes, but more barlenses than mine. 28% of barred galaxies in their sample hosted X-shapes or barlenses, corresponding fairly well with my 31%. They found a flat axial ratio distribution for the combined sample of barlenses and X-shapes, contrasting my findings here, which give a high peak in edge-on galaxies as shown by figure 30. Additionally they found

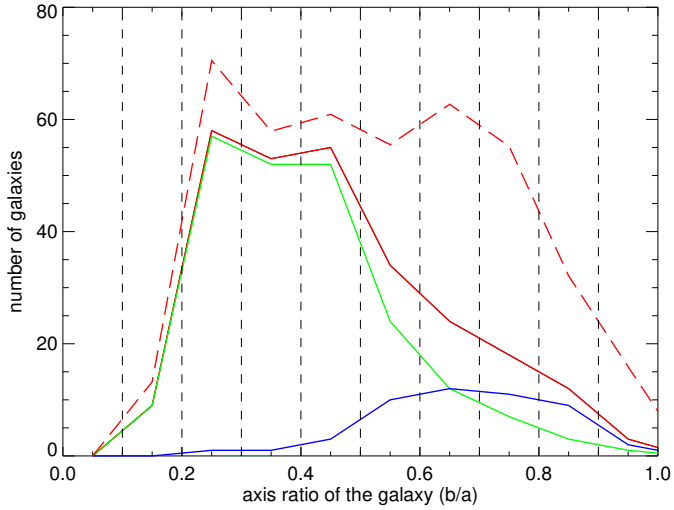

Figure 30: The minor-to-major axis ratio distribution of galaxies with barlenses or X-shapes. The green line shows X-shapes, the blue line barlenses, and the solid red line them both together. The dashed red line shows the distribution of all galaxies scaled by a factor of 0.3. The sample is plotted in 0.1 axis ratio bins.

that in the Hubble type distribution, X-shapes have a peak at around T=+1 and barlenses at around T=-1, while in my sample both seemed to have the peak at around T=+1, thus showing more X-shapes in lenticulars (figure 24).

In the sample used by Laurikainen et al. (2014) the S^{4}G galaxies were selected by their blue magnitudes, angular diameters and radial velocities, and NIRS0S galaxies by their magnitudes, Hubble types and inclinations ($-3 < T < 1$; $i < 65°$), while my sample was limited only by the galaxy angular diameter and area of the sky. While the differences in the sample criterion make direct comparison of the results difficult, some things are still interesting to note. I found much less barlenses than X-shapes, contrasting the nearly equal amounts found by Laurikainen et al. This also explains the differences in the axial ratio distributions of the galaxies, as more X-shapes means a peak in high galaxy inclinations (figure 21).

While barlenses are a rather recently discovered structure, there has been many studies on the prevalence of B/P bulges among edge-on galaxies. It should be noted that not all B/P bulges necessarily have X-shapes visible in their unsharp masked images, and as such a dedicated search might find more B/P bulges from my sample. As B/P bulges are generally thought of as edge-on structures, it makes sense to limit any comparisons to edge-on galaxies only. My sample had 33/171 X-shapes or barlenses in galaxies with inclination higher than 75°. That is 19%

fraction with a 6% margin of error.

Lütticke, Dettmar, & Pohlen (2000) found a B/P bulge in 45% of edge-on disc galaxies. Their sample consisted of 1343 high inclination disc ($-3.5 < T < +9.5$) galaxies, chosen by diameter from the Third Reference Catalogue of Bright Galaxies (RC3; de Vaucouleurs et al. 1991). They identified the B/P bulges by eye from contour plots of the galaxies classifying them in three categories: peanut-shaped bulges (1), box-shaped bulges (2), and close to box-shaped bulges (3). As their classification relied on contour plots, and they did not look for X-shapes, it is unsurprising that they found much higher fractions than I. However, taking only their B/P bulges of types 1 and 2, which made up little less than half of the total fraction, gives a fraction of about 20%, which is nearly identical to that of my sample.

Yoshino & Yamauchi (2014) found 22% fraction of B/P bulges in their sample of 1329 nearby edge-on galaxies. They used a diameter and magnitude limited sample taken from SDSS DR7. The identification of B/P bulges was done by eye using residual images. They divided the B/P bulges into three categories bx+, bx, and bx-, with X-shapes visible only in bx+ and bx type bulges. They found X-shapes in only about 10% of their sample. They used the single-epoch SDSS release images, compared to my use of the deeper co-adds by Fliri & Trujillo. The angular size limit of their sample was $r_{petrosian} > 10$ arcsec [3], compared to my $D25 > 30$ arcsec. Additionally, they did the identification with residual images created in a different manner to my unsharp masked images. As such, it is possible that they missed some weak X-shapes in their analysis due to lesser quality of their images, the smaller size of their galaxies and due to different image treatment.

The fraction of interacting galaxies in my sample was 14.9%, that of mergers 2.1%, and that of peculiars 2.3%. This means that 19.2% of the galaxies in the sample were experiencing, or had recently experienced, some sort of interaction. The comparison to other studies is somewhat difficult, as the indicators of interaction are not well defined in literature, and the concepts "merger" and "interacting galaxy" vary greatly between different works.

Miskolczi et al. (2011) searched for minor mergers in 474 galaxies from the SDSS DR7 archive. They looked for tidal features caused by accretion of smaller companions, such as streams, in galaxies with no nearby massive companions. They found faint tidal features in up to 19% of their sample galaxies, with. 6% showing distinct stream like features. These numbers are high compared to mine as they did not search for major mergers or interactions between massive galaxies. They divided the found features in four categories according to how clear the features were, with only their category III (making up bit under third of the

[3] $r_{petrosian}$ is a radius calculated by setting the local intensity of light at the radius equal to some constant times the average intensity of light within the radius (Petrosian, 1976).

features) having galaxies where the features could be caused by interaction with massive companion. As such, most of the features they found would fall under my category "peculiar", with possibly some mergers in all their categories and interacting galaxies in III. Their sample excluded ellipticals, face-on galaxies and galaxies with diameter less than two arcminutes, so it is not surprising that they found more minor mergers than I.

Hood et al. (2018) found tidal features with high confidence level in 17% of the galaxies, and hints of them in up to 29% of the galaxies, in their sample of 1048 galaxies selected from the Resolved Spectroscopy of a Local Volume (RESOLVE) survey. They searched for streams, shells, tails and arms and did not exclude galaxies with clear massive companions like Miskolczi et al. (2011) did. The RESOLVE survey is volume limited, spanning two equatorial strips RESOLVE-A and RESOLVE-B, both bounded with the Local Group-corrected heliocentric velocity between $V_{LG} = 4500 - 7000$ km/s. RESOLVE-A spans $8.75 < R.A. < 15.75$ hr and $0° < Dec. < 5°$, while RESOLVE-B covers the same area as Stripe 82. The agreement with my data is very good, considering the imprecision of the detection of tidal features.

Morales et al. (2018) found 14% fraction of faint tidal features indicative of minor mergers in their sample of 297 Local Volume ($v_r < 2000$ km/s) S^4G galaxies. They searched for only minor mergers, and excluded all known major mergers from their final sample. In that sense their fraction is again quite high compared to mine, though part of it may be explained by sample selection effects and differences in classification of the tidal features.

Duc et al. (2015) found evidence of tidal interactions in half of their sample of 92 early type galaxies, though they make no claims of completeness. They divided interacting galaxies to three, physically motivated categories (in addition to non-interacting fully relaxed galaxies and undetermined galaxies): minor merges, major mergers and interacting galaxies. They called minor mergers galaxies that had a regular halo with streams or shells, arguing these to be caused by the accretion of low-mass companions. Galaxies with strongly perturbed halo, dust lanes, tidal tails and no massive companion were defined as major merger. Interacting meant in their scheme a galaxy with a perturbed halo and prominent tails with a massive companion. In my classification scheme I would have called their major mergers as peculiars, their minor mergers as peculiars or ongoing mergers, and their interacting galaxies as ongoing mergers or interacting galaxies. Their fraction of minor mergers was 16%, major mergers 12% and interacting galaxies 22%. The $ATLAS^{3D}$ sample they used is limited by distance (less than 42 Mpc), morphological type (early type), and absolute K-band magnitude (brighter than -21.5). Additionally, the sub-sample used was biased towards low to medium density environments, high galaxy masses, extended galaxies, slow rotators and gas-rich objects.

My sample appears to have quite a low number of minor mergers in particular. It is of course possible that many of the galaxies I classified as interacting galaxies could be interpreted as past minor mergers instead, due to the uncertainty of diagnosing interaction between two visually close galaxies. Other reason for this could be that still deeper imaging would be required to find the faint low surface brightness tidal features from the most far-away galaxies of my sample.

4.2.2 Image quality

My sample was limited only by apparent diameter (larger than 0.5 arcminutes) and area of the sky (Stripe 82), and as such it contains many relatively faint and far-away galaxies. While the resolution of the images was mainly sufficient, for some galaxies it was at the limit for recognizing internal features such as barlenses and X-shapes (figure 31 shows examples), and possibly also for external low surface brightness features. Also, the angular diameter distribution of the X-shapes and barlenses (figure 32), shows that the fraction of barlenses and X-shapes grows with the angular diameter. As such it is very likely that some barlenses and X-shapes were missed, and the actual number of them and B/P bulges in the sample is higher than what was found. This is especially true for barlenses, since while X-shapes are still relatively easy to find from the unsharp masks of even fairly faint and far-away galaxies, barlenses are more difficult to identify. This can be even seen in the figure 32, with the peak of the barlens fraction located in larger angular diameters than that of X-shapes. Figure 33 shows that the minor-to-major axis ratio of the galaxies hosting barlenses or X-shapes becomes much flatter while looking at only visually large galaxies. This probably explains some of the discrepancy of the number of barlenses found compared to that of X-shapes in relation to Laurikainen et al. (2014).

Figure 32 also shows the angular diameter distribution of the fraction of interacting galaxies. While the relation is not as clear as for X/bl features, there is a peak in large diameters for the interacting galaxies. Some indicators of interaction could have been missed in the faintest and furthest away galaxies. As expected, there is no such relation for mergers and peculiars, which differ from regular galaxies to such degree that there is no difficulty in identifying them in any of the galaxies of my sample.

The same co-addition treatment that preserves the low surface brightness features in distant galaxies, also preserves intra-galactic features, such as the galactic cirrus, as can be seen in figure 34. Galactic cirrus is starlight scattered off by dust grains in the diffuse interstellar medium (Elvey & Roach, 1937). When studying extra-galactic objects, this is of course unwanted, as it can obstruct the view to the targets, and could even be mistaken for stellar streams or other low surface brightness features in target galaxies. Luckily the cirrus is usually easy to distinguish

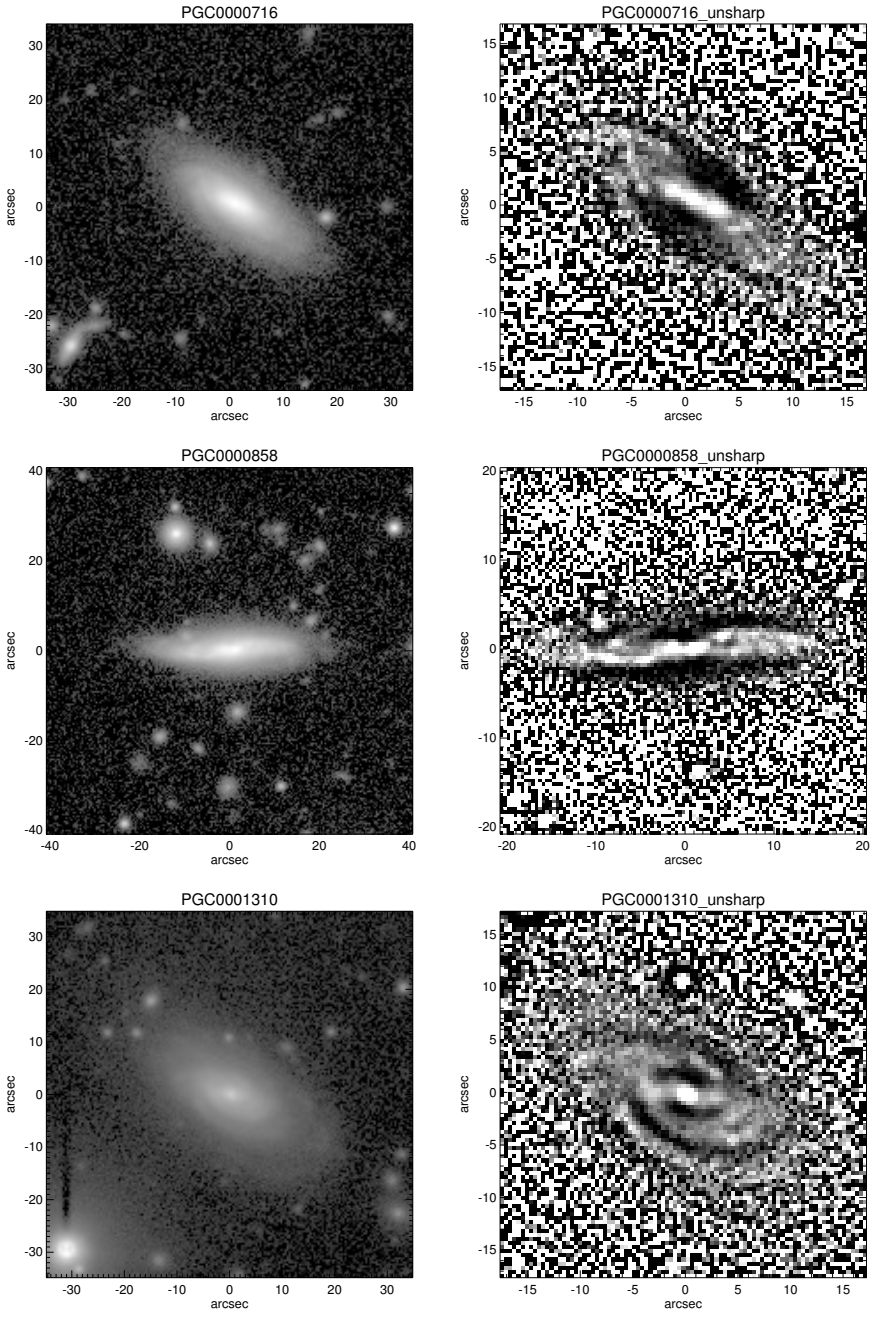

Figure 31: PGC0000716 (upper row), PGC0000858 (middle row), and PGC0001310 (bottom row). These galaxies were classified as not having X-shapes or barlenses. Each however have hints of them in their morphologies, and could reveal them if higher resolutions were available. Images are in *i*-band.

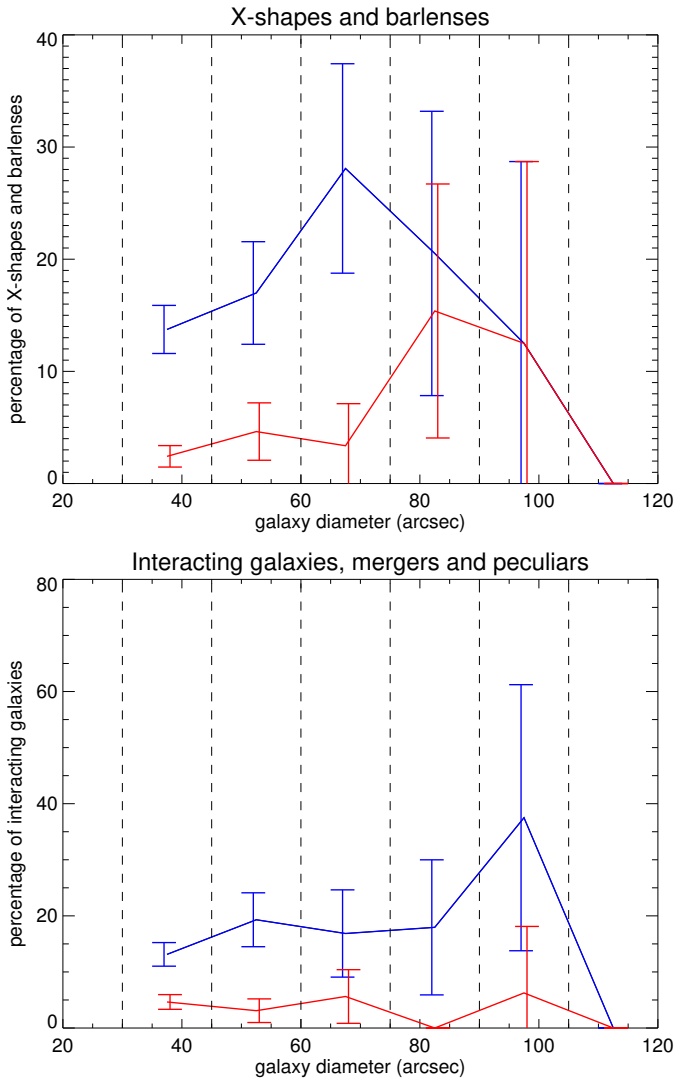

Figure 32: The angular diameter distribution of X/bl features, as well as that of interacting galaxies and mergers and peculiars. The upper plot shows X-shapes in blue and barlenses in red, while the lower plot shows interacting galaxies in blue and mergers and peculiars in red. Note the different y-axes. There is a clear relation between the angular diameters and the X/bl fractions, especially for barlenses. A less clear relation is also present for interacting galaxies. The sample is plotted in 15 arcsecond bins.

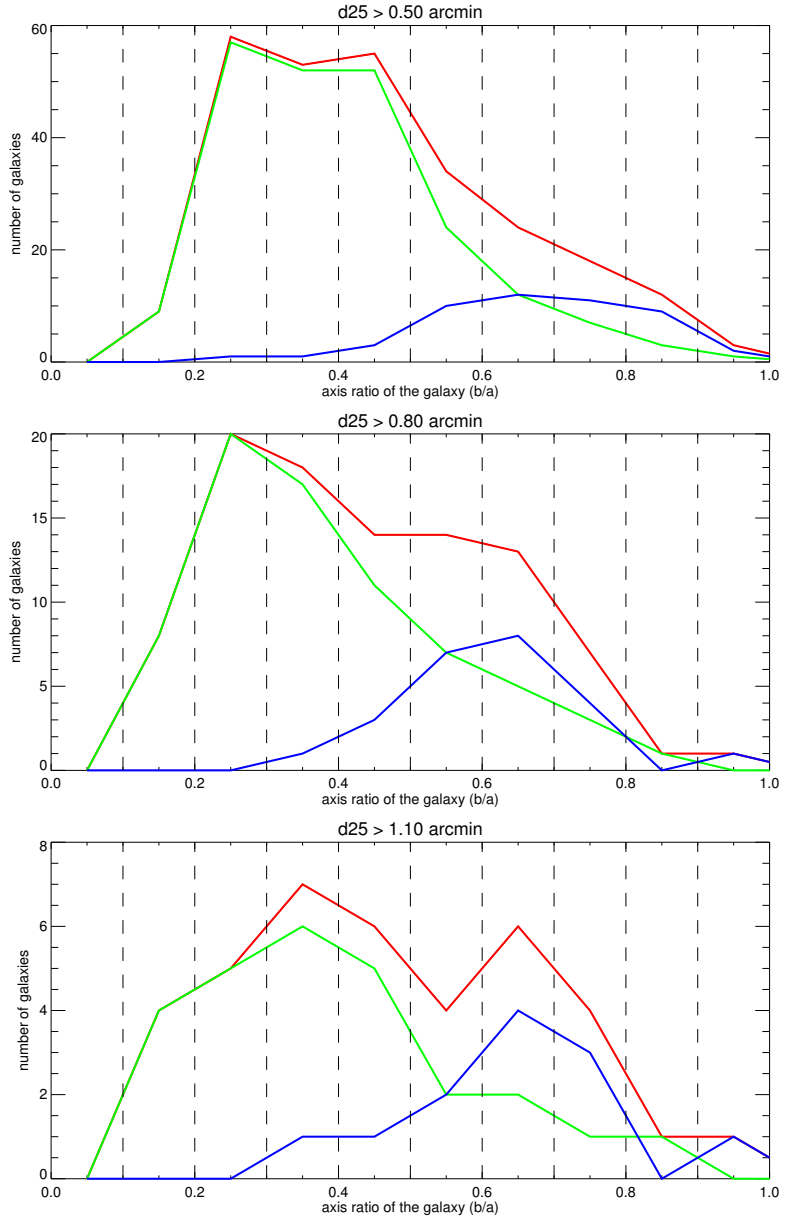

Figure 33: The minor-to-major axis ratio distributions for galaxies with barlenses and X-shapes. The upper plot shows the whole sample (266 galaxies with a barlens or an X-shape), the middle only the galaxies with angular diameter greater than 0.8 arcminutes (96 galaxies with a barlens or an X-shape) and the lower only the galaxies with angular diameter greater than 1.1 arcminutes (38 galaxies with a barlens or an X-shape). The green line shows the X-shapes, the blue the barlenses and the red both. Among visually larger galaxies, the amount of barlenses approaches that of X-shapes.

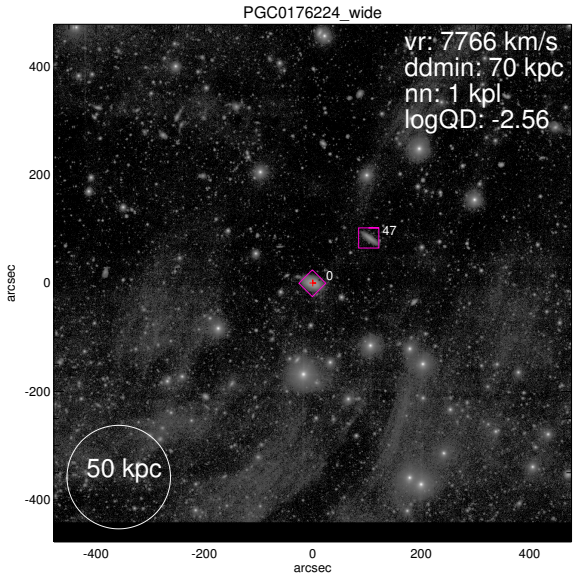

Figure 34: Galactic cirrus around PGC0176224. The cirrus is especially clear in the lower part of the image. Image is in the 'ultra-deep *r*-band'.

from actual structures, and as such it should not affect the statistics of the sample, much like the random contamination by Milky Way stars.

4.2.3 Source catalogs

My results can only be as reliable as the source catalogs and databases that I use. This is somewhat an issue as for many faint and far-away galaxies, which there are many in the sample, only fairly rough data exists.

For many galaxies clearly visible in the images, no redshift data exist. This makes the search for possible interacting companions of the sample galaxies difficult, as there is no way to tell whether a galaxy is only a visual pair and actually is a fore- or background object, or if they are actually physically related. This is especially problematic when there are slight disturbances in the sample galaxy morphology, which could easily be caused by internal effects. It can be expected that the real number of interacting galaxies in the sample is higher than the one I present here.

Most of the sample galaxy data that was not measured by myself, was taken from HyperLEDA, including axial ratios and Hubble types. HyperLEDA collects its data from numerous different surveys and measurements, and although its data is homogenized, it is not always entirely reliable, especially for not well studied objects. This can be seen in the amount of barlenses and X-shapes I found in pre-

sumably unbarred galaxies: 5 barlenses and 118 X-shapes (18 of which were clear X-shapes) in 941 galaxies claimed as unbarred by HyperLEDA. This presents an inherent and hard to measure error in my data.

4.3 Future work

As barlenses are a relatively recently discovered structure, there is still much research to be done about them and their relation to interactions. Simulations as well as observational studies are required to build a satisfactory scheme for their formation and evolution.

Many of the results I have presented here, could have interesting implications, but are not statistically significant, and as such require further study with better statistics to confirm or deny. One of those is the different relation to interaction by barlenses and X-shapes, barlenses being more common and X-shapes rarer in interacting galaxies (table 2). Another one is the inclination dependence of the X-shapes in interacting galaxies (figure 20).

Mergers and peculiars would be an especially interesting topic to study, as one would expect that the catastrophic merging events they have undergone would destroy any non-relaxed structure such as X/bl features. Yet this is not necessarily the case as proven by the four merger/peculiar X-shape hosting galaxies I found, especially PGC1151183. To gain any useful statistics about B/P structures in these very strongly interacting galaxies, a more dedicated sample would be required.

Another avenue of further research would be that of more specified classification of interaction and merger properties. It is clear from my results that all interactions do not have the same effect on B/P structures. Specifying whether a merger is minor or major, wet or dry, could reveal different behaviors. An example of another, possibly better classification scheme of interacting galaxies would be that of Duc et al. (2015).

Deeper surveys with higher resolutions will always ease the detection of morphological structures, and allow better statistics when studying their prevalence. Other way to improve the statistics is the development of image treatment methods such as unsharp masks to highlight specific features. Unsharp masking already allows X-shapes to be detected very easily from even faint, low resolution galaxies. For future studies requiring statistics of B/P structures, I would focus on improving the detection of barlenses, for example by using isophotal contour plots. I feel this would result in a more complete and representative sample than the one I present here.

5 Summary and conclusions

In this thesis I studied the effects of interactions on X/bl structures in a sample of 1413 galaxies located in the Stripe 82. Using the deep co-adds by Fliri & Trujillo (2016), I identified interactions as well as X/bl structures in the galaxies. Redshifts from several catalogs were used in the search for interacting companions, while unsharp masks were created for the *i*-band co-adds for the identification of the X-shapes.

Using statistical analysis I compared the X-shape and barlens distributions in interacting galaxies, as well as in merger/peculiar galaxies to those of non-interacting galaxies. I examined the inclination, absolute magnitude, and Hubble type distributions of the X/bl features. I obtained the following results:

1. In the sample of 1413 galaxies I found 217 X-shapes and 49 barlenses. This is a high but reasonable number of X-shapes and a low number of barlenses compared to previous studies. I suspected that I may have missed some barlenses in my sample due to the difficulty of identifying them in the most poorly resolved galaxies of my sample.

2. There is a statistically significant deficiency of X-shapes among massive interacting galaxies. In Milky Way luminosity and brighter edge-on galaxies ($M_{abs} < -21$ and $i > 60°$) there is X-shapes in only fifth of the interacting galaxies, compared to the nearly half of the non-interacting galaxies. I suggested that this may be linked with the gas properties of the galaxies, and how they are affected by interactions.

3. In general, interacting galaxies hosted slightly less X-shapes than non-interacting galaxies, with X-shapes present in $13\% \pm 5\%$ of interacting galaxies and in $16\% \pm 3\%$ of the non-interacting galaxies. No such relation was found for barlenses, and barlenses were even slightly more common in interacting galaxies at $5\% \pm 3\%$ occurrence level, compared to the $3\% \pm 2\%$ occurrence level in the non-interacting galaxies. However, the differences were not statistically significant.

4. The inclination distribution for X-shapes differed slightly for interacting and non-interacting galaxies, with less X-shapes in high inclination interacting galaxies and more in low inclination interacting galaxies. This means that low inclination X-shapes react to interactions similarly to barlenses. I speculated that this may be caused by differences in the robustness of the face-on and edge-on structures of the X/bl structures.

5. Two ongoing merger galaxies out of 29 hosted X-shapes, as well as two peculiar galaxies out of 32. No merger or peculiar galaxies hosted barlenses.

The numbers were too low for mergers and peculiars to gain any useful statistics, though even the existence of any X-shapes among them speaks for the robustness of the feature. This is the case especially for PGC1151183, which seems to have undergone a recent major merger.

In conclusion, I feel that it is safe to say that there is no simple answer to the question 'What is the effect of interaction on B/P bulges?' The answer will depend on the properties of the interaction, and also on those of the parent galaxies. To fully understand the relation of interactions and mergers to B/P/X/bl structures, more work on the subject is required.

A Catalog

Image catalog of the 1413 galaxies of the sample can be found in the web at `www.oulu.fi/astronomy/STRIPE82/stripe82_index.html`. The catalog is split into 14 categories according to interaction and X/bl features of the galaxies (mostly same as table 1). For each galaxy there are three images: an unsharp masked *i*-band image, a wide field 'ultra-deep *r*-band' image with nearby companions marked on it, and a regular *i*-band image. These are the same images as explained in section 2. A screenshot from the catalog is shown in figure 35. Additionally, an IDL (Interactive Data Language) save file containing all the parameters used for the statistical analysis can be found at the site.

References

Abazajian, K. N., Adelman-McCarthy, J. K., Agüeros, M. A., et al. 2009, The Astrophysical Journal Supplement Series, 182, 543

Athanassoula, E. 2003, in Astrophysical Supercomputing using Particle Simulations, ed. J. Makino & P. Hut, Vol. 208, 177

Athanassoula, E. 2005, Monthly Notices of the RAS, 358, 1477

Athanassoula, E. 2016, in Galactic Bulges, ed. E. Laurikainen, R. Peletier, & D. Gadotti, Vol. 418, 391

Athanassoula, E., & Bosma, A. 1985, Annual Review of Astronomy and Astrophysics, 23, 147

Athanassoula, E., Laurikainen, E., Salo, H., & Bosma, A. 2015, Monthly Notices of the RAS, 454, 3843

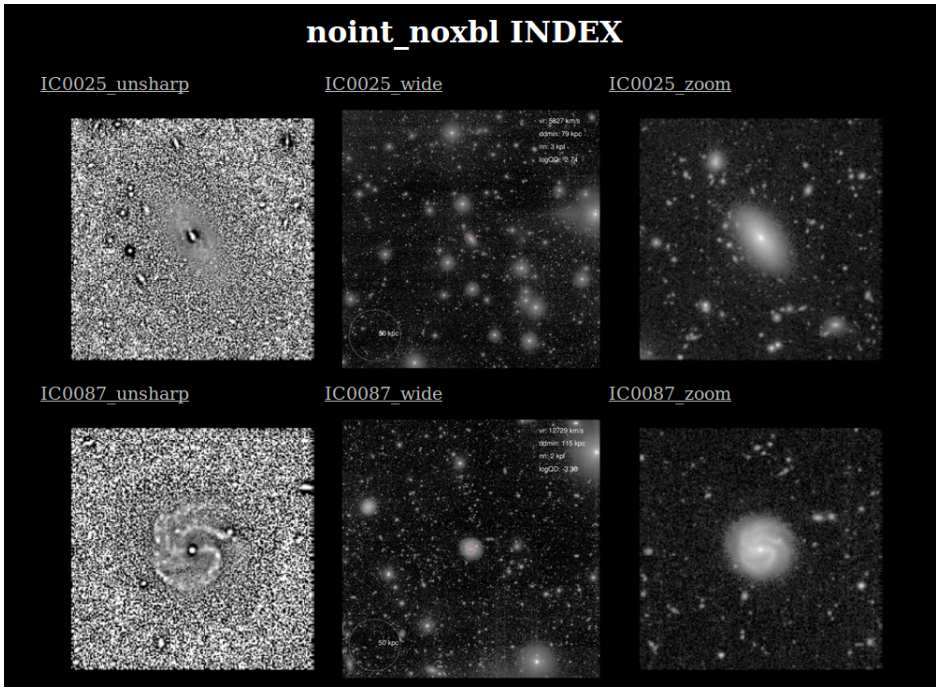

Figure 35: A screenshot from the catalog website, from the category 'Non-interacting galaxies without X/bl features'. The unsharp masked *i*-band images are at left, the wide field 'ultra-deep *r*-band' images in the middle, and the regular *i*-band images at right.

Blanton, M. R., Kazin, E., Muna, D., Weaver, B. A., & Price-Whelan, A. 2011, Astronomical Journal, 142, 31

Bureau, M., Aronica, G., Athanassoula, E., et al. 2006, Monthly Notices of the RAS, 370, 753

Combes, F., & Sanders, R. H. 1981, Astronomy and Astrophysics, 96, 164

Dahari, O. 1984, Astronomical Journal, 89, 966

de Vaucouleurs, G., de Vaucouleurs, A., Corwin, Herold G., J., et al. 1991, Third Reference Catalogue of Bright Galaxies

Duc, P.-A., & Renaud, F. 2013, Tides in Colliding Galaxies, ed. J. Souchay, S. Mathis, & T. Tokieda, 327

Duc, P.-A., Cuillandre, J.-C., Karabal, E., et al. 2015, Monthly Notices of the RAS, 446, 120

Eggen, O. J., Lynden-Bell, D., & Sandage, A. R. 1962, Astrophysical Journal, 136, 748

Elvey, C. T., & Roach, F. E. 1937, Astrophysical Journal, 85, 213

Few, J. M. A., & Madore, B. F. 1986, Monthly Notices of the RAS, 222, 673

Fliri, J., & Trujillo, I. 2016, Monthly Notices of the RAS, 456, 1359

Hernquist, L., & Quinn, P. J. 1988, Astrophysical Journal, 331, 682

—. 1989, Astrophysical Journal, 342, 1

Herrera-Endoqui, M., Salo, H., Laurikainen, E., & Knapen, J. H. 2017, Astronomy and Astrophysics, 599, A43

Hood, C. E., Kannappan, S. J., Stark, D. V., et al. 2018, Astrophysical Journal, 857, 144

Huchra, J. P., Vogeley, M. S., & Geller, M. J. 1999, The Astrophysical Journal Supplement Series, 121, 287

Kormendy, J., & Illingworth, G. 1982, Astrophysical Journal, 256, 460

Laurikainen, E., & Salo, H. 2017, Astronomy and Astrophysics, 598, A10

Laurikainen, E., Salo, H., Athanassoula, E., Bosma, A., & Herrera-Endoqui, M. 2014, Monthly Notices of the RAS, 444, L80

Laurikainen, E., Salo, H., Buta, R., & Knapen, J. H. 2011, Monthly Notices of the RAS, 418, 1452

Laurikainen, E., Salo, H., Laine, J., & Janz, J. 2018, Astronomy and Astrophysics, 618, A34

Li, Z.-Y., Ho, L. C., & Barth, A. J. 2017, Astrophysical Journal, 845, 87

Licquia, T. C., Newman, J. A., & Brinchmann, J. 2015, Astrophysical Journal, 809, 96

Łokas, E. L., Ebrová, I., del Pino, A., et al. 2016, Astrophysical Journal, 826, 227

Lütticke, R., Dettmar, R. J., & Pohlen, M. 2000, Astronomy and Astrophysics Supplement Series, 145, 405

Makarov, D., Prugniel, P., Terekhova, N., Courtois, H., & Vauglin, I. 2014, Astronomy and Astrophysics, 570, A13

Mihos, J. C., Walker, I. R., Hernquist, L., Mendes de Oliveira, C., & Bolte, M. 1995, Astrophysical Journal, 447, L87

Miskolczi, A., Bomans, D. J., & Dettmar, R. J. 2011, Astronomy and Astrophysics, 536, A66

Moetazedian, R., Polyachenko, E. V., Berczik, P., & Just, A. 2017, Astronomy and Astrophysics, 604, A75

Morales, G., Martínez-Delgado, D., Grebel, E. K., et al. 2018, Astronomy and Astrophysics, 614, A143

Nair, P. B., & Abraham, R. G. 2010, The Astrophysical Journal Supplement Series, 186, 427

Noguchi, M. 1987, Monthly Notices of the RAS, 228, 635

Pan, H.-A., Lin, L., Hsieh, B.-C., et al. 2018, ArXiv e-prints, arXiv:1810.10162

Paturel, G., Fouque, P., Bottinelli, L., & Gouguenheim, L. 1989, Astronomy and Astrophysics Supplement Series, 80, 299

Petrosian, V. 1976, Astrophysical Journal, 210, L53

Pettitt, A. R., & Wadsley, J. W. 2018, Monthly Notices of the RAS, 474, 5645

Salo, H., & Laurikainen, E. 2017, Astrophysical Journal, 835, 252

Sérsic, J. L. 1963, Boletin de la Asociacion Argentina de Astronomia La Plata Argentina, 6, 41

Sheth, K., Regan, M., Hinz, J. L., et al. 2010, Publications of the Astronomical Society of the Pacific, 122, 1397

Skokos, C., Patsis, P. A., & Athanassoula, E. 2002, Monthly Notices of the RAS, 333, 847

Toomre, A. 1977, in Evolution of Galaxies and Stellar Populations, ed. B. M. Tinsley & D. C. Larson, Richard B. Gehret, 401

Toomre, A. 1981, in Structure and Evolution of Normal Galaxies, ed. S. M. Fall & D. Lynden-Bell, 111–136

Toomre, A., & Toomre, J. 1972, Astrophysical Journal, 178, 623

Wall, J. V., & Jenkins, C. R. 2003, in Practical statistics for astronomers, by J.V. Wall and C.R. Jenkins. Cambridge observing handbooks for research astronomers, vol. 3. Cambridge, UK: Cambridge University Press, 2003, 93

White, S. D. M., & Rees, M. J. 1978, Monthly Notices of the RAS, 183, 341

Yoshino, A., & Yamauchi, C. 2014, ArXiv e-prints, arXiv:1410.8262

Zana, T., Dotti, M., Capelo, P. R., et al. 2018, Monthly Notices of the RAS, 473, 2608